

RESEARCH ARTICLE

MS23, a master basic helix-loop-helix factor, regulates the specification and development of the tapetum in maize

Guo-Ling Nan^{1,**}, Jixian Zhai^{2,3}, Siwaret Arikit^{2,*}, Darren Morrow¹, John Fernandes¹, Lan Mai^{1,‡}, Nhi Nguyen^{1,§}, Blake C. Meyers^{2,¶} and Virginia Walbot^{1,**}

ABSTRACT

Successful male gametogenesis involves orchestration of sequential gene regulation for somatic differentiation in pre-meiotic anthers. We report here the cloning of *Male Sterile23* (*Ms23*), encoding an anther-specific predicted basic helix-loop-helix (bHLH) transcription factor required for tapetal differentiation; transcripts localize initially to the precursor secondary parietal cells then predominantly to daughter tapetal cells. In knockout *ms23-ref* mutant anthers, five instead of the normal four wall layers are observed. Microarray transcript profiling demonstrates a more severe developmental disruption in *ms23-ref* than in *ms32* anthers, which possess a different bHLH defect. RNA-seq and proteomics data together with yeast two-hybrid assays suggest that MS23 along with MS32, bHLH122 and bHLH51 act sequentially as either homo- or heterodimers to choreograph tapetal development. Among them, MS23 is the earliest-acting factor, upstream of bHLH51 and bHLH122, controlling tapetal specification and maturation. By contrast, MS32 is constitutive and independently regulated and is required later than MS23 in tapetal differentiation.

KEY WORDS: Pre-meiotic male reproduction, Regulatory hierarchy, Transcriptome, Proteome

INTRODUCTION

Maize is monoecious, with separate inflorescences producing female-only ears and male-only tassels on the same plant. Tassels contain hundreds of florets, each with three stamens, compound organs consisting of a slender filament subtending an anther, a four-lobed organ in which meiosis occurs followed by pollen development. A relatively large size, the 30-day-long period of anther development, and the regularity of ontogeny in which anther length allows accurate developmental staging have facilitated dissection and confocal reconstruction of cell division and expansion patterns in maize anthers (Kelliher and Walbot, 2011). Additionally, there are hundreds of male-sterile mutants (Skibbe and Schnable, 2005) including a subset disrupting somatic lobe

development prior to meiosis (Timofejeva et al., 2013; Egger and Walbot, 2016). These maize resources were developed in part to facilitate hybrid seed production using male-sterile plants as ear parents with pollen supplied by a male-fertile partner line. These mutants are also a rich genetic resource to define steps in anther ontogeny.

The tapetum (TP) plays sequential, essential roles in anthers, ferrying nutrients to pre-meiotic cells and later the pollen mother cells (PMCs) and the meiocytes, remodeling the extracellular callose coating of the PMCs and tetrads, and secreting exine onto maturing pollen grains. As tapetal cells senesce, their collapsing walls form a landing pad to which the uninucleate pollen must attach (Kelliher and Walbot, 2011; Tsou et al., 2015). Mutations in numerous genes exhibit tapetal defects from pre- to post-meiosis (Timofejeva et al., 2013).

The bHLH transcription factors (TFs) in flowering plants consist of large families with 213 encoding genes annotated in maize (Lin et al., 2014), 178 in rice and 170 in *Arabidopsis* (Carretero-Paulet et al., 2010). Mutant analysis demonstrates that several tapetal bHLHs are crucial for (1) pre-meiotic to meiotic stages: *Arabidopsis* *DYSFUNCTIONAL TAPETUM1* (*DYT1*) (Zhang et al., 2006; Feng et al., 2012), its rice homolog *UNDEVELOPED TAPETUM1* (*UDT1*) (Jung et al., 2005), and the maize homolog, *Male Sterility32* (*Ms32*) (Moon et al., 2013); rice *ETERNAL TAPETUM1* (*EAT1* – OS04G0599300, also named *DELAYED TAPETUM DEGENERATION* or *DTD*) (Niu et al., 2013; Ji et al., 2013); rice *TDR INTERACTING PARTNER2* (*TIP2* – OS01T0293100; also named *bHLH142*) (Fu et al., 2014; Ko et al., 2014); *Arabidopsis* *bHLH10*, *bHLH89* and *bHLH91* (Zhu et al., 2015); as well as for (2) meiotic to post-meiotic stages: *Arabidopsis* *ABORTED MICROSPORES* (*AMS*) (Sorensen et al., 2003; Xu et al., 2010, 2014) and its rice homolog *TAPETUM DEGENERATION RETARDATION* (*TDR*) (Li et al., 2006; Zhang et al., 2008).

A tapetal cell arises from periclinal division of a bipotent precursor, the secondary parietal cell (SPC). In the *ms23-ref* mutant, pre-tapetal initials conduct an extra periclinal division generating a defective double layer (Chaubal et al., 2000). This complete bilayer is unique, because other mutants exhibit irregular periclinal divisions. The epidermis (EP), endothecium (EN) and middle layer (ML) appear normal cytologically in *ms23-ref*, whereas the tapetal cells lack a dense cytoplasm and are not binucleate, two characteristics of normal TP during meiosis; the meiocytes in *ms23-ref* fail to progress beyond meiotic prophase I. We report here the cloning of the bHLH encoded by *Ms23* and demonstrate that its transcript accumulates in the SPC before TP formation and then reaches much higher levels as tapetal cells differentiate. We elucidate the distinct and overlapping processes regulated by MS23 and a second bHLH, MS32, and propose a sequential deployment and hierarchy of four tapetal bHLHs. Finally, we contrast the maize pattern with that of related bHLHs in rice and *Arabidopsis*.

¹Department of Biology, Stanford University, Stanford, CA 94305, USA.

²Department of Plant and Soil Sciences and Delaware Biotechnology Institute, University of Delaware, Newark, DE 19716, USA. ³Department of Biology, South University of Science and Technology, Shenzhen 518055, China.

*Present address: Rice Science Center, and Department of Agronomy, Faculty of Agriculture, Kasetsart University, Kamphaeng Saen, Nakhon Pathom 73140, Thailand. †Present address: North American Science Associates, Inc., 9 Morgan, Irvine, CA 92618, USA. ‡Present address: 603 Old Farm Road, Valhalla, NY 10595, USA. §Present address: Donald Danforth Plant Science Center, 975 Warson Road, St. Louis, MO 63132, USA.

**Authors for correspondence (gnan@stanford.edu; walbot@stanford.edu)

© G.-L.N., 0000-0002-1286-0249; J.Z., 0000-0002-7906-4976; S.A., 0000-0002-2964-1886; J.F., 0000-0002-2445-8273; B.C.M., 0000-0003-3436-6097; V.W., 0000-0002-1596-7279

RESULTS

Confocal analysis of cytological defects in *ms23-ref* mutant anthers

Using confocal images with an established stage numbering convention as a guide (Kelliher et al., 2014), the changing cytology of the *ms23-ref* mutant was compared with its fertile counterpart across key stages of anther development (Fig. 1A). We examined three axes: *x* (width), *y* (length) and *z* (depth) (Fig. 1B). At Stage 4 – the three-wall-layer stage shortly after a periclinal division of the primary parietal cells (PPCs) generated EN and the SPC – *ms23-ref* and fertile siblings were indistinguishable. At Stage 7, about half of the bipotent SPCs had divided periclinally, with a complete four-

wall-layered lobe formed by Stage 8. The periclinal divisions of both PPCs and SPCs appeared normal in *ms23-ref* anthers, in terms of initiation timing and completion of a four-layer anther wall. In fertile anthers, the pre-meiotic archesporial cells completed mitotic divisions before Stage 9, then matured into the PMCs; these synthesized DNA and organized the meiotic chromosomes then entered prophase I, progressed through zygotene, and entered meiosis II at Stages 8, 9 and 10, respectively (Nan et al., 2011). During the pre-meiotic and meiotic stages, somatic wall layer cells continued to divide anticlinally to add anther width and length.

Starting at Stage 8 there were extra periclinal divisions in *ms23-ref* (Fig. 1A). At Stage 9, ~75% of the lobe had an extra

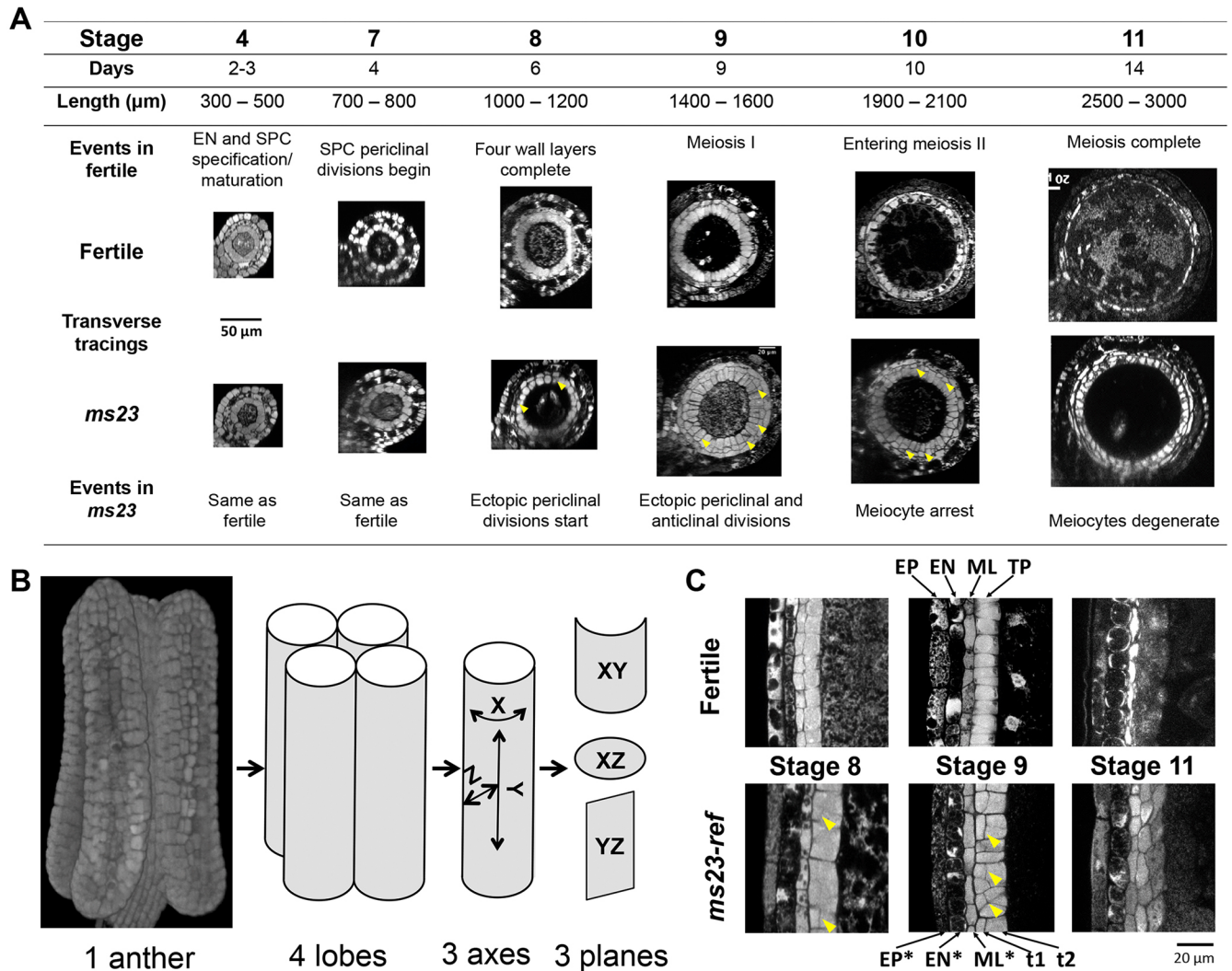


Fig. 1. Key stages of anther development in the *ms23-ref* male sterile mutant and its fertile sibling. (A) Transverse confocal sections (*xz* plane) of fertile and *ms23-ref* sterile anthers categorized by length and timing of cell type events. Stage 4 (300–500 μm): EN and SPCs are specified with three wall layers completed in fertile anthers; Stage 7 (700–800 μm): the periclinal divisions of SPCs are more than halfway completed to generate ML and TP; Stage 8 (1000–1200 μm): fertile pollen mother cells prepare to enter prophase I whereas ectopic periclinal divisions are observed in *ms23-ref*; Stage 9 (1400–1600 μm): fertile meiocytes in prophase I and *ms23-ref* have an ~80% complete extra layer; Stage 10 (1900–2100 μm): fertile germinal cells at meiosis II and a >90% complete extra layer is formed and meiocytes degenerate in *ms23-ref*; Stage 11 (~3000 μm): meiosis is complete and tetrads form in fertile anthers whereas meiocytes collapse completely in *ms23-ref*. Previously, Stage 5 (500 μm) designated the timing of the first periclinal division in the secondary parietal layer in the W23 inbred line, and Stage 6 was 500–700 μm , a period in which approximately 50% of the SPCs divide periclinally (Kelliher et al., 2014). The number of days is referenced to the onset of anther initiation. (B) The *x* (width), *y* (length) and *z* (depth) axes examined in maize anther lobes. (C) Longitudinal confocal images of *ms23-ref* anthers at three developmental stages. Anther wall layers (outer to inner) in fertile anthers: EP, epidermis; EN, endothecium; SPCs, secondary parietal cells; ML, middle layer; TP, tapetum. The asterisk designation is used for the layers in similar positions in *ms23-ref*: EP*, the presumptive epidermis; EN*, the presumptive endothecium; ML*, the presumptive middle layer; t1, the aberrant fourth wall layer; t2, the aberrant fifth layer (Chaubal et al., 2000). Yellow arrowheads point to cells produced by extra periclinal division.

periclinal division; these cells were vacuolated and often irregularly shaped with oblique walls rather than the regular architecture of cuboidal, densely cytoplasmic cells found in fertile TP (Kelliher and Walbot, 2011). The aberrant fourth and fifth innermost layers are termed t1 and t2 (Fig. 1C) as previously described (Chaubal et al., 2000). At Stage 10, both t1 and t2 cells had similar shapes and sizes viewed in the *xy* plane (Fig. S1). However, the outer ring of t1 cells were thinner in the *z*-dimension, resembling the ML in fertile anthers, whereas the inner t2 layer had a greater *z*-dimension, closer to the TP in fertile anthers (Fig. S1).

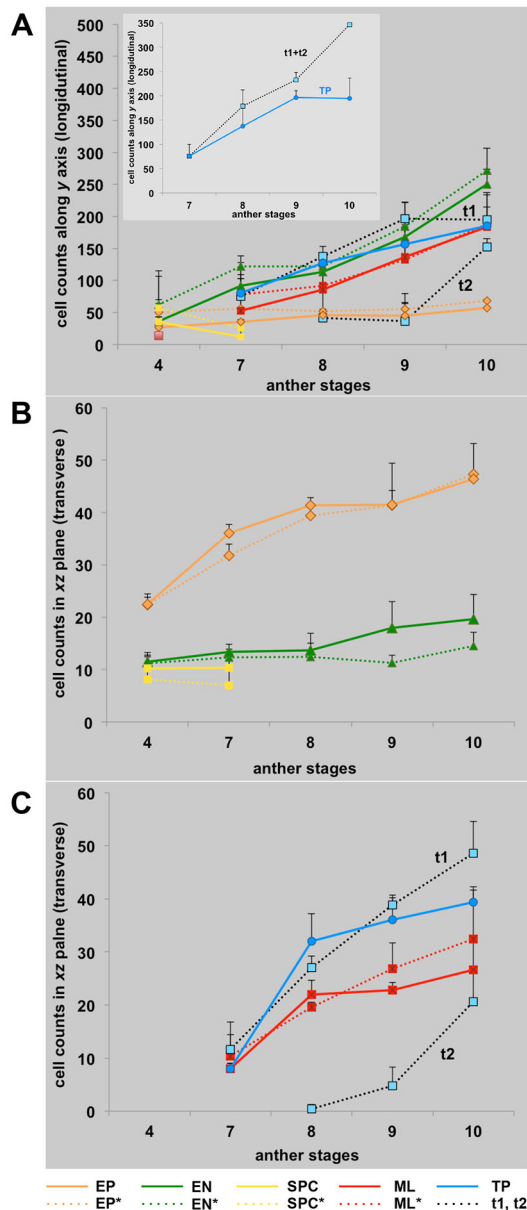


Fig. 2. Anther cell count data from confocal images. (A) Cell counts in a column along the *y* axis. (B) Cell counts of EP/EP*, EN/EN* and SPC/SPC* in the *xz* plane (transverse section). (C) Cell counts of ML/ML* and TP, t1 and t2 in the *xz* plane. In fertile anthers: EP, epidermis; EN, endothecium; ML, middle layer; TP, tapetum. In *ms23-ref* anthers: EP*, the presumptive epidermis; EN*, the presumptive endothecium; ML*, the presumptive middle layer; t1, the fourth layer; t2, the fifth layer. Fertile data points are plotted as a solid line with sterile sibling data as dotted lines. Error bars represent s.d.

Using cell count data, we further analyzed the division patterns in *ms23-ref* (Fig. 2). Because mutant anthers continued to elongate and lobes expanded, it was not surprising to see continuous length- and girth-adding anticlinal divisions. The divisions along the *y* axis of EP* (the outermost, EP-like first layer), EN* (the EN-like second layer), and ML* (the ML-like third layer) in *ms23-ref* were similar to EP, EN and ML in fertile anthers, respectively (Fig. 1C; Fig. 2A). The cell count data of the t1 layer resembled those of the TP until Stage 8 when t2 appeared. To examine the girth-adding anticlinal divisions, we viewed the *xz* plane and observed similar cell counts before Stage 8 across all four wall-layers but some cell types soon deviated (Fig. 2B,C). Although anticlinal divisions of fertile tapetal cells along the *x* axis slowed after Stage 8, the aberrant t1 cells maintained the same pace of cell division and t2 cells appeared from ectopic periclinal divisions (Fig. 2C). By Stage 10, the t1 layer had conducted significantly more anticlinal divisions than normal TP ($P=0.049$). In *ms23-ref*, the cell counts along the *x* axis of EP*, SPC* (the SPC-like third layer during the three-wall-layer stage) and ML* did not show significant differences, but the mutant EN* exhibited a significantly reduced rate of anticlinal divisions, particularly at Stage 9 ($P=0.041$) (Fig. 2B,C).

Map-based cloning of the *Ms23* gene

ms23-ref was a historic, unmapped recessive male-sterile mutant. Using bulk segregation analysis, *Ms23* was initially placed on both chromosomes 6 and 8 (Fig. S2). PCR markers flanking the two implicated regions were tested and confirmed the male sterility phenotype to co-segregate with polymorphic markers near bins 8.00–8.01 on chromosome 8. Thirty recombinants were found after surveying >250 sterile plants from several 1:1 homozygous male-sterile/heterozygous fertile populations segregating the *ms23-ref*, *ms23-6027* or *ms23-6059* alleles. *Ms23* placement was within 0.75 Mb of the end of chromosome 8S. RNA-seq data for the 15 gene models in this region were retrieved from qTeller (<http://qTeller.com>); only GRMZM2G021276, spanning positions 95,823 to 98,367 and encoding a predicted bHLH protein, showed tassell-specific expression (Fig. S3). Tiling PCR primer pairs were employed to identify allele-specific lesions (Fig. 3; Fig. S4). In *ms23-ref*, the entire gene is deleted; this deletion encompasses up to 96.5 kb defined by retention of the two closest annotated genes and their transcripts: GRMZM2G122850 at 67.4–71.3 kb and GRMZM2G081127 at 167.8–168.8 kb (data not shown). *ms23-6027* is a frameshift allele with a 2-bp (AT) insertion at position 1076, causing an early termination codon at position 1091 immediately upstream of the predicted bHLH region (Fig. 3; Fig. S4A). The *ms23-6059* allele has a 4-bp (GCTC) insertion, 13 bases after the predicted translation initiation site (Fig. 3).

As annotated in Maize B73 RefGen_v3, the 2361 bp *Ms23* gene is confirmed to have four exons. cDNA prepared from fertile W23 anthers validated a 1619-nt primary transcript with an initiation

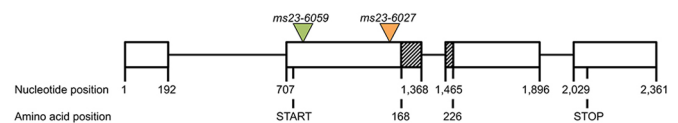


Fig. 3. Structure of *Ms23* alleles. There are four exons; the start codon (ATG) at nucleotide 775 is in exon 2, and the stop codon is in exon 4 at nucleotide 2100. The bHLH domain (striped box) encompasses amino acid positions 168 to 226 spanning the second intron (1278 to 1548). The *ms23-ref* allele is null, because the entire gene is deleted; the *ms23-6027* and *ms23-6059* alleles contain frameshift mutations caused by insertions at cDNA positions 1077 (orange triangle, AT) and 769 (green triangle, GCTC), respectively.

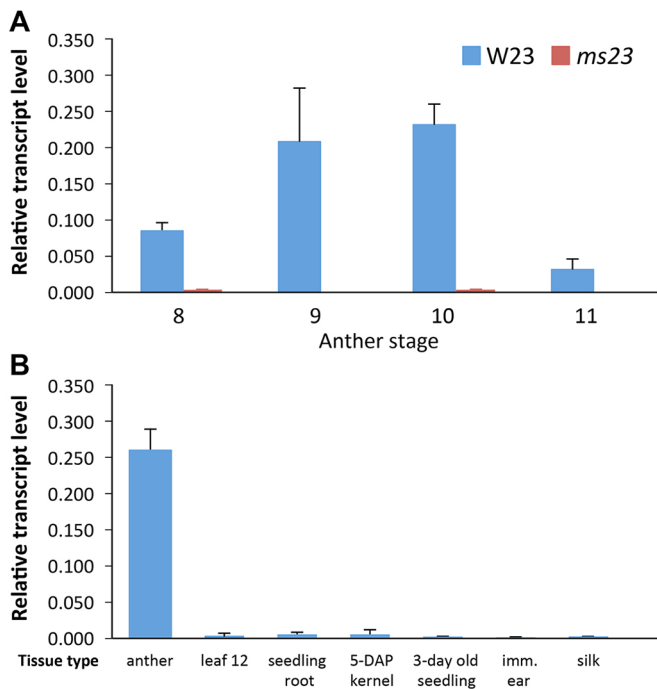


Fig. 4. Quantitative RT-PCR analysis of *Ms23* expression. (A) *Ms23* transcript levels in W23 wild-type (blue) and *ms23-ref* mutant (red) anthers from Stages 8 to 11. (B) *Ms23* expression in diverse organs compared with Stage 10 anthers. Expression values were normalized to the cyanase gene (Ma et al., 2007). Error bars represent s.d. DAP, days after pollination; imm. ear, immature ear before pollination.

codon in the second exon at nucleotide position 775 and a termination codon at position 2098 in the fourth exon (Fig. 3). It encodes a 365 amino acid predicted bHLH (<http://grassius.org/grasstfdb.html>) with at least one predicted nuclear localization signal motif, PRATGRGRKR, at amino acid residues 146–155 with a cutoff score at 0.6 (<http://www.moseslab.csb.utoronto.ca/NLStradamus/>; Nguyen Ba et al., 2009).

Ms23 expression

To understand better the spatiotemporal scope of *Ms23* action, quantitative RT-PCR (qRT-PCR) was performed on successive stages of W23 fertile anthers and other organs. *Ms23* expression

reached its peak at Stage 10 (Fig. 4A); it was undetectable (or near the limit of detection) in all other samples (Fig. 4B). By RNA-seq, *Ms23* transcript was detectable in anthers before Stage 4 at 200 and 400 μm (Zhai et al., 2015), and the levels rose steadily, peaking around Stage 10, after which it gradually decreased.

By *in situ* hybridization (Fig. 5), *Ms23* transcript was detected in the SPCs and both daughter cells (pre-ML and pre-TP) immediately after the periclinal division (Stage 7). However, the PMCs had a patchy signal; the callose coat appeared to trap probe, and we considered the signal to be an artifact (Zhang et al., 2014). Within a day, when SPC daughters diverge morphologically into distinctive cell shapes, *Ms23* signal intensity was reduced in the maturing ML (Fig. 5). From Stages 8 to 9, *Ms23* transcripts predominated in the TP (Fig. 5). Loss of *Ms23* signal in the ML, later enrichment in the TP, and a 10-fold increase at Stage 10 compared with Stage 7 indicate that although the SPC expresses *Ms23*, there was a substantial increase specifically in the differentiating TP (Fig. 5). Either transcript stability or transcription or both were reduced in the ML. No antisense transcript was detected with a sense probe in the control (Fig. 5A, inset).

Many bHLH proteins are associated with tapetal development

Using the MS23 protein sequence, many related genes were identified in angiosperms (Fig. S5; <http://www.gramene.org/>). Phylogenetic relationships of these bHLHs in maize, rice and *Arabidopsis* (Fig. 6) and a multiple sequence alignment of bHLH domains (Fig. S6) suggest that there has been conservation of regulatory networks for tapetal development.

MS23 and its paralog bHLH122 fall in clade A along with two rice proteins, TIP2 and EAT1 (Fig. 6). TIP2 is the rice ortholog of MS23, sharing 72.68% similarity in the full-length protein and 91.11% within the bHLH domain (Table S1). Maize bHLH122 is the ortholog of rice EAT1. In *Arabidopsis*, there are three clade A orthologs, bHLH10, bHLH89 and bHLH91, which are stamen specific and appear to act redundantly (Zhu et al., 2015). Maize bHLH51, rice TDR and *Arabidopsis* AMS, all in the B clade, are larger proteins, ranging from 551 to 625 amino acids, with 74.6% similarity in the bHLH domain (Fig. S6). *Ms32*, the other historical maize mutant with tapetal periclinal divisions (Chaubal et al., 2000) and high expression in the TP (Moon et al., 2013), encodes a protein that falls into clade C along with rice UDT1 and *Arabidopsis* DYT1 (Fig. 6).

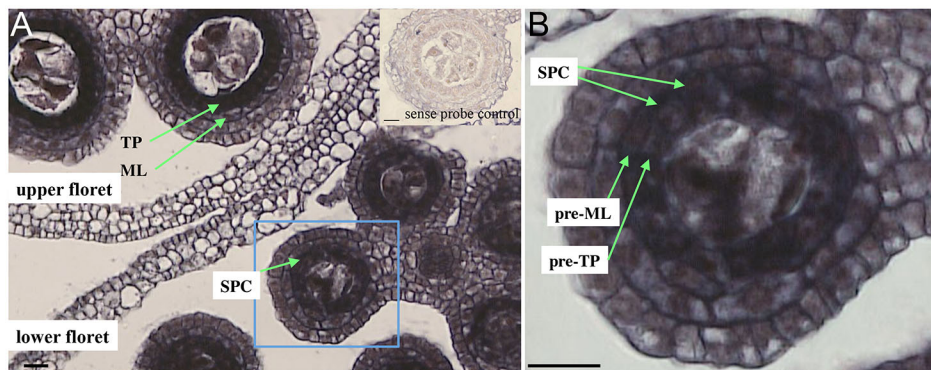


Fig. 5. RNA *in situ* hybridization in anther transverse section. (A) In each maize spikelet, there are two florets, i.e. the developmentally more advanced, adaxial upper floret and the younger abaxial lower floret. Shown is transcript detection by hybridization with an *Ms23* antisense probe at Stage 7 in the lower floret when the last round of periclinal divisions in fertile anthers are in progress and at Stage 9 in the upper floret when all four wall layers of anthers are complete. SPC, secondary parietal cells; pre-ML, pre-middle layer initials; pre-TP, pre-tapetal initials; ML, middle layer cells; TP, tapetal cells. Inset shows negative control with a Stage 9 anther hybridized with an *Ms23* sense probe. (B) The boxed region in A, viewed at a higher magnification, showing SPCs alongside the pre-ML and pre-TP. Scale bars: 20 μm .

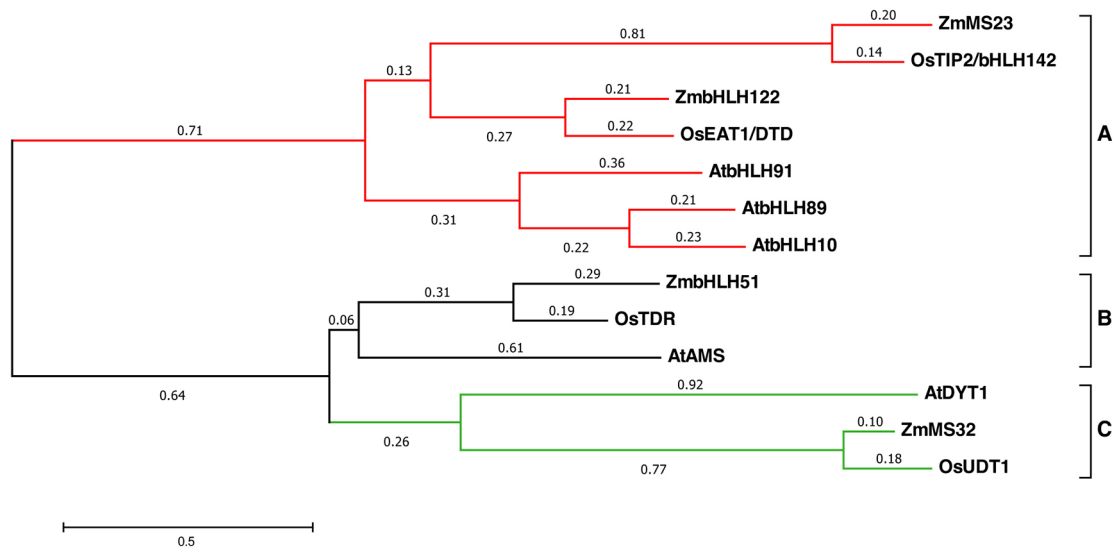


Fig. 6. Phylogenetic analysis of tapetal bHLHs from maize (*Zm*), rice (*Os*) and *Arabidopsis* (*At*). The evolutionary analysis was conducted in MEGA6 using the maximum likelihood method based on the Poisson correction model. The tree with the highest log likelihood is shown. Initial tree(s) for the heuristic search were obtained by applying the neighbor-joining method to a matrix of pairwise distances estimated using a JTT model. The tree is drawn to scale, with branch lengths depicting the rate of substitutions per site with a total of 774 positions in the final dataset involving 13 amino acid sequences. Three clades (A,B,C) are defined with the A versus B, C clade diverging first.

Microarray profiling of *ms23-ref* and *ms32* anthers

The *ms23-ref* and *ms32* transcriptomes were compared with those of fertile siblings to quantify gene expression patterns. To analyze the differentially expressed genes, only the probes detected at Stage 9 in both mutant and fertile anthers were further analyzed ($n=24,682$) at the criteria of 1.5-fold difference and $P \leq 0.05$. More genes were affected in *ms23-ref* (1236 up, 1293 down) compared with *ms32* (520 up, 866 down) (Fig. 7). The shared, differentially regulated set accounted for a smaller portion (24%) in *ms23-ref* compared with those (44%) in *ms32* (Fig. 7). The severely downregulated class showed greater fold change than those upregulated (Fig. S7). For example, there were over three times (217 down versus 61 up) and seven times (88 down versus 12 up) more downregulated genes in the *ms23-ref* anthers at the 4-fold and 8-fold change criteria, respectively (Fig. S7). The *ms32* transcriptome showed a similar trend with over four times (126 down/26 up) and approximately six times (59 down/10 up) more downregulated genes at the 4- and 8-fold change criteria,

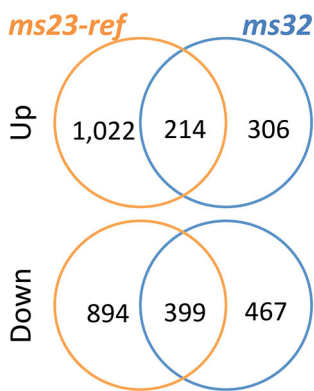


Fig. 7. Differentially expressed genes. Up- or downregulated genes detected by microarray hybridization at the 1.5-fold change criterion ($P \leq 0.05$) in 1500 μm (Stage 9) *ms23-ref* and *ms32* anthers compared with their respective fertile siblings.

respectively. We conclude that MS23 and MS32 are transcriptional activators in most contexts because there are more substantial defects in gene activation than in repression.

At the 4-fold criterion, more than half of the genes examined ($n=75$; Table S2) were downregulated in both *ms23-ref* and *ms32*, which demonstrated that both bHLHs were required to activate one or more common downstream pathways. There were 64 genes downregulated only in *ms23-ref* and 30 only in *ms32* (Table S2). Seven genes annotated with TF activity and two associated with hormone homeostasis were on the *ms23-ref*-specific list, indicative of discrete pathways controlled by MS23, independently of MS32. Considering the earlier required action in pre-tapetal cells (and possibly SPCs) of MS23 and the large number of genes that are misregulated in *ms23-ref* anthers, the absence of MS23 had a greater impact on anther gene expression than did absence of MS32 (Fig. 7). Intriguingly, the *Dcl5* gene (responsible for a type of floral-specific phasiRNAs) was about 16-fold lower in both mutants compared with their fertile counterparts, demonstrating that both bHLHs were required for 24-nt phasiRNA biogenesis (Fig. S8; Zhai et al., 2015).

MS23 is a master regulator in maize anthers

Normalized abundances of RNA-seq reads were obtained from published data spanning ten stages from 200 to 5000 μm of W23 anthers (Zhai et al., 2015). Selecting the ten most abundant bHLH transcripts at each stage yielded 23 genes. *Ms23*, *bHLH51* and *bHLH122* were in the top ten across the 1500 to 3000 μm stage whereas *Ms32* expression was lower with less fluctuation (Table S3; Fig. 8). *Ms23* transcript peaked at 2000 μm , nestled between two bursts of *bHLH122* at 1500 and 2500 μm ; *bHLH51* was the most abundant bHLH transcript type in meiotic (2000 μm) through uninucleate microspore (3000 μm) stages. As most other bHLH transcripts subsided post-meiotically, *Ms32* exceeded all but *bHLH51* in anthers at the 5000 μm stage, shortly before pollen shed (Fig. 8).

To explore global transcripts in *ms23-ref* anthers, we conducted deep sequencing (RNA-seq) at 400-, 700-, 1000-, 1500- and 2000- μm stages in the original ND101 background. The near invariant cyanase (GRMZM2G134747) transcript (Ma et al., 2007) was used

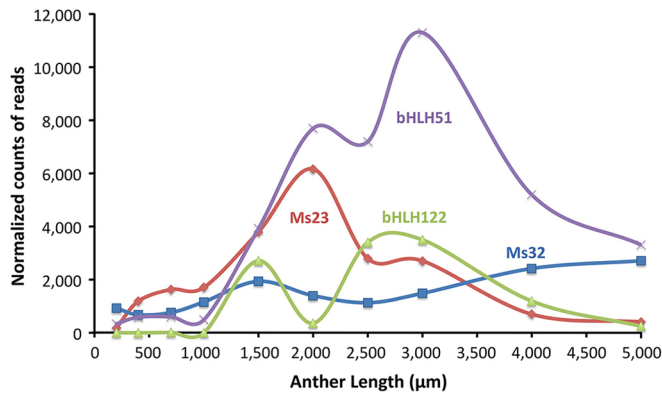


Fig. 8. Expression patterns of *Ms23*, *Ms32*, *bHLH51* and *bHLH122*. The total counts of RNA-seq reads in each gene model are normalized to 10 million reads (TP10M) (Zhai et al., 2015).

as an internal normalization standard to compare the RNA-seq data between the W23 fertile and *ms23-ref* libraries. Many TFs were misregulated in *ms23-ref* anthers (Table S4). Using a 2-fold criterion, 28% of the bHLH class ($n=58$), 30% of MYB ($n=50$), 30% of bZIP ($n=39$) and 16% of MADS ($n=12$) TFs were affected (Table S4). About 40% ($n=63$) showed a 4-fold or greater difference ($\log_2 \leq -2$ or $\log_2 \geq 2$). The data not only validated *ms23-ref* as a true null allele but also expanded the list of bHLHs either positively or negatively regulated by MS23. In 1500- μm *ms23-ref* anthers, *bHLH122* was almost undetectable and *bHLH51* was down 12-fold, indicating that their expressions were dependent on MS23 (Fig. S9). These differences were validated with qRT-PCR (data not shown).

By contrast, *Ms32* expression was slightly up (~ 3.7 -fold) in *ms23-ref* at 2000 μm when there were about twice as many TP-like cells ($t1+t2$) in *ms23-ref*, indicating that *Ms32* could be expressed in these aberrant cells in the absence of MS23. qRT-PCR results substantiated these findings and further illustrated that expression of *Ms32* was somewhat delayed in *ms23-ref* (Fig. S10A). Although *bHLH122* expression was lower in *ms32* anthers at Stage 9, neither *Ms23* nor *bHLH51* was affected (Fig. S10B).

The expression patterns of all 213 maize bHLHs across these five anther stages in both fertile and *ms23-ref* plants were analyzed with algorithms from the Cluster 3.0 program (<http://bonsai.hgc.jp/~mdehoon/software/cluster/>). An average linkage heat map of hierarchical gene clustering based on Euclidean distance showed a tight correlation (0.96) between *Ms23* and *bHLH51* (Fig. S11). *bHLH122* was also associated with *Ms23* and *bHLH51* (0.28) whereas *Ms32* was dissimilar (0.00).

Pathway analysis (<http://pathway.gamene.org/maizecyc.html>) further illustrated many downstream cellular processes, including secondary metabolism, hormone biosynthesis/degradation, transporters, respiration/energy alteration, and lipid/fatty acid metabolism, were affected across Stages 4-10 in the *ms23-ref* anther (Fig. S12). In particular, the hormone pathways were notably altered (Table S5), also validating the array data of a tassell-specific dihydroflavonol-4-reductase gene (GRMZM2G168893) in the brassinosteroid pathway (Table S2).

Distinct protein expression patterns

Trypsin-digested protein samples from W23 fertile anthers at Stages 8 and 10 plus pollen were analyzed by HPLC-MS/MS. MS23 and bHLH51 were abundant proteins at Stage 10 but not at Stage 8 (Table 1). bHLH122 protein was below the detection limit at both stages, consistent with the RNA-seq result that the transcript levels

Table 1. Proteomic data corroborate the RNA-seq results

A. Proteomics – spectral counts						
Protein	W23 anther length					
	1.0 mm	2.0 mm	Pollen			
MS23	n.d.	284	n.d.			
MS32	279	363	1311			
bHLH51	n.d.	730	n.d.			
bHLH122	n.d.	n.d.	n.d.			
B. RNA-seq transcript abundance (normalized)						
Gene	W23 anther length					
	1.0 mm	1.5 mm	2.0 mm	2.5 mm	3.0 mm	Pollen
<i>Ms23</i>	1713	3800	6163	2798	2708	0
<i>Ms32</i>	1164	1942	1400	1136	1488	164
<i>bHLH51</i>	494	3926	7691	7195	11,294	3
<i>bHLH122</i>	4	2712	364	3406	3500	0

The relative spectral abundance of each protein analyzed by HPLC-MS/MS was normalized as described by Facette et al. (2013). RNA-seq data are from W23 fertile anthers (Zhai et al., 2015). n.d., not detectable.

were low at both stages, bracketing a spike at Stage 9. These results suggested that there could be stage-specific deployment and rapid turnover across a 3-day span. As expected from its constitutive RNA expression, MS32 was found in both Stage 8 and 10 anthers and was highly abundant in pollen (Table 1). MS32 is a widely expressed protein detected in leaves (Facette et al., 2013) and transcripts are found in multiple organs (Fig. S13; https://mpss.danforthcenter.org/dbs/index.php?SITE=maize_RNAseq).

Protein and genetic interactions

Using yeast two-hybrid assays, the interactions among the bHLH domains of MS23, MS32, bHLH51 and bHLH122 were tested. All possible combinations of interactions, including all negative controls, were examined. Strong interactions occurred with co-transformation of MS23+bHLH51, MS32+bHLH122, bHLH51+bHLH122, and bHLH51+bHLH51 (Fig. S14). Other homodimers and heterodimers were either weak or not detected consistently.

We generated *ms23-ref*, *ms32* double-mutant plants for cytological studies. Confocal images showed additivity with the first extra periclinal division observed around Stage 8, similar to the timing of the *ms23-ref* single mutant, and multiple extra layers, a typical phenotype of *ms32*, were found in the double mutant at Stage 11 (Fig. S15). Both the protein interactions and the genetic data support the model of sequential actions of MS23 and MS32 in separate pathways during tapetal differentiation, with a later common cascade during TP degeneration.

Impact of TP defects on small RNA biogenesis

There is a drastic decrease in *Dcl5* (formerly *Dcl3b*) transcripts in *ms23-ref*; DCL5 is required to generate 24-nt phasiRNAs and, as expected, these are virtually eliminated in *ms23-ref* (Fig. S8; Zhai et al., 2015). In *mac1* and *msca1* mutants, both lacking the TP (Wang et al., 2012; Chaubal et al., 2003), the miR2275 trigger molecules for 24-phasiRNA biogenesis are nearly undetectable (Zhai et al., 2015). miR2275 is present in *ms23-ref*; however, the 24-PHAS precursor transcripts are drastically reduced (Zhai et al., 2015). A data re-analysis indicated that *ms23-ref* accumulated an abnormal distribution of miR2275 types (Fig. S16). In fertile anthers, there was a single dominant member of the family (*zma-miR2275b-5p*), representing $\sim 40\%$ of all the subtypes and about 50 times more abundant than *zma-miR2275b-3p* in 1000- μm anthers (Fig. S16). In *ms23-ref*, diverse miR2275 species were present: in

order of abundance, the expected zma-miR2275b-5p, zma-miR2275a-3p, zma-miR2275b-3p, zma-miR2275c-3p and zma-miR2275a-5p (Fig. S16). We conclude that the mature miRNAs of the miR2275 family are not accumulating normally in the t1 and t2 of *ms23-ref* anthers. With altered miR2275 composition and near elimination of both 24-*PHAS* precursors and *Dcl5* transcripts in *ms23-ref* anthers, MS23 plays a direct or indirect role in the biogenesis of 24-phasiRNAs.

DISCUSSION

Bipotent SPCs undergo periclinal divisions in both fertile and *ms23-ref* mutant anthers (Fig. 1). By Stage 8, when periclinal divisions complete, fertile tapetal cells have a dense cytoplasm, but extra periclinal divisions start in *ms23-ref* anthers to make t1 and t2 layers. Neither t1 nor t2 develops into the TP. Our interpretation of the *ms23-ref* phenotype is that the SPCs are defective and generate pre-tapetal daughters that can divide anticleinally to sustain anther growth but can also recapitulate the secondary parietal program of periclinal division. By contrast, *ms32* anthers appear normal at Stage 8 with all four wall-layers specified, including the ML and TP; at Stage 9, the extra periclinal divisions start (Fig. S15). Therefore, MS23 is crucial for regulation of the bipotent stem cell activity of SPC to specify the ML and TP and is crucial for early tapetal differentiation steps; MS32 is essential for restricting cell divisions and growth after the tapetal cells are specified and most anticlinal divisions have finished. *Ms23* expression is independent of *Ms32*. *Ms32* expression is elevated at Stage 10 in *ms23-ref* anthers compared with fertile siblings, a pattern that we conclude is an indirect effect of the increased number of pre-tapetal cells in *ms23-ref*.

Mutants of *tip2*, the rice ortholog of *Ms23*, have sporadic, periclinal divisions in the pre-tapetal layer but never form a complete bilayer as in *ms23-ref* (Fu et al., 2014; Ko et al., 2014). Furthermore, *in situ* hybridization reveals that transcript localizations are distinct in these grasses. *Ms23* is detected in the SPC and both the daughter cells immediately after periclinal division, followed by a rapid reduction in the ML, with persistent and increased tapetal expression. The expression of *Ms23* in the ML is transitory and might reflect only pre-existing, SPC-derived transcripts. In rice, *TIP2* transcripts are in the ML and TP as well as weakly present in the EN when all four wall layers are present (Fu et al., 2014). Interestingly, in maize, the initial site of the lower signal in the ML is restricted along the lobe circumference; it constitutes a stripe along the outer arc along the length of each lobe. This arc location is precisely where *Ocl4* b-ZIP TF transcripts and

miR2118 molecules are located in the EP (Wang et al., 2012; Vernoud et al., 2009; Zhai et al., 2015). One role of OCL4 is to repress periclinal divisions in the EN from Stages 4 to 7, presumably through a mobile signal (Wang et al., 2012). We hypothesize that this outer epidermal arc might also act instructively to promote cell commitment and differentiation in the ML, some aspect of which is counter-regulated by MS23.

No mutants for maize *bHLH122* or *bHLH51* are available; however, *bHLH122* transcription is highly dependent on MS23, placing it downstream of *Ms23*, similar to its rice ortholog *EAT1* (Niu et al., 2013). *bHLH51* is likely to be more important later during pollen development similar to its rice *TDR* and *Arabidopsis AMS* orthologs based on its peak expression after Stage 11 (Fig. 8).

Maize *ms32* and the orthologous rice *udt1* mutants share the phenotype of ectopic periclinal divisions; however, there are no extra periclinal divisions observed in the orthologous *Arabidopsis dyt1* mutant. In all three species, the cells in the anomalous 'TP' expand tremendously in the z-dimension and may crush the arrested meiocytes; the post-meiotic terminal phenotypes of meiocyte failure and pollen abortion are likely consequences of earlier defects in lobe ontogeny arising from aberrant periclinal divisions of tapetal cells. Because maize anthers are much larger and develop more slowly (Kelliher et al., 2014), we determined that *Ms32* is constitutively expressed starting in early lobe ontogeny, but there are no obvious cytological defects until Stage 9. *Arabidopsis DYT1* is expressed across the *Arabidopsis* anther stages 4-7 (Feng et al., 2012), which corresponds to Stages 4-11 in maize and the rice anther stages 4-8 (Table S6; Sanders et al., 1999; Zhang and Wilson, 2009; Kelliher et al., 2014). Furthermore, *Ms32* is expressed in many maize organs (Fig. S13), although there are no mutant phenotypes noted outside of anthers. Therefore, MS32 is likely to be functionally redundant with other bHLHs in most contexts. Similarly, rice *UDT1* is found in diverse organs whereas *TIP2*, the ortholog of *Ms23*, is mainly restricted to the inflorescence (http://ensembl.gamene.org/genome_browser/index.html).

Despite conservation of bHLHs important in tapetal development, mutant studies demonstrate distinctive features of the gene hierarchy, time of action, and mutant phenotypes of four bHLHs (Fig. 9). In maize and rice, the two clade A genes (*Ms23* and *bHLH122*, and *TIP2* and *EAT1*) are functionally distinctive (and in rice both are required for fertility) whereas in *Arabidopsis*, there are three copies of clade A genes (*bHLH10*, *bHLH89* and *bHLH91*) and only triple mutants exhibit sterility (Zhu et al., 2015). Maize *Ms23* (rice *TIP2*) controls expression of both *bHLH51* (rice *TDR*) and *bHLH122* (rice

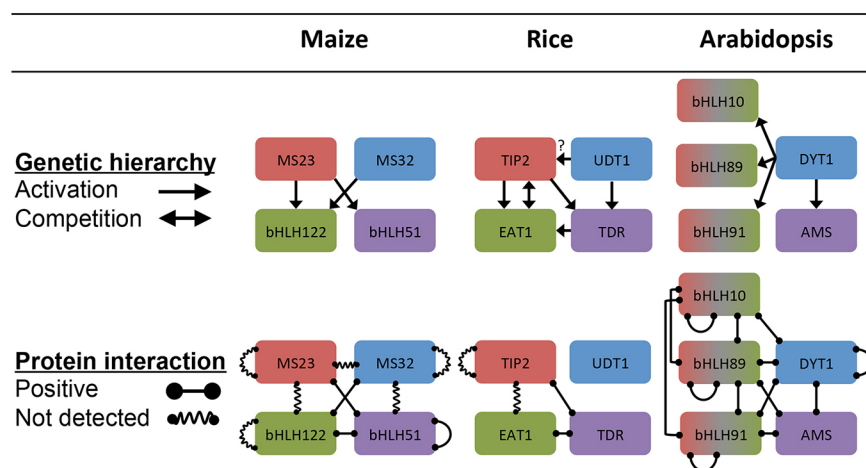


Fig. 9. Genetic networks of the tapetal bHLHs in maize, rice and *Arabidopsis*. Interactions of bHLHs in maize tapetal development contrasted with rice and *Arabidopsis*. Maize MS23 (red), bHLH122 (green), MS32 (blue) and bHLH51 (purple) are depicted with rice and *Arabidopsis* homologs in the same color scheme. The partially redundant *Arabidopsis* gene family of bHLH10, bHLH89 and bHLH91 are shown in mixed red-green boxes. Solid lines indicate positive interactions, and wiggly lines indicate no detected interactions; single arrows indicate activations, double arrow indicates competition.

EAT1) (Fig. S10). By contrast, rice *EAT1* positively regulates the expression of *TIP2* (Ko et al., 2014). *Arabidopsis AMS* is regulated by *bHLH10*, *bHLH89* and *bHLH91*. *Ms32* is upstream of *bHLH122* but does not directly regulate the expression of either *Ms23* or *bHLH51*. In rice, the ortholog of *Ms32* (*UDT1*) is upstream of both *EAT1* and *TDR*. In *Arabidopsis*, the ortholog of *Ms32* (*DYT1*) is also upstream of *bHLH10*, *bHLH89*, *bHLH91* and *AMS*. Interestingly, *Ms32*, *UDT1* and *DYT1* are all upregulated in the mutants corresponding to *ms23-ref* (rice *tip2* and *Arabidopsis bhlh10/bhlh89/bhlh91*) (Fu et al., 2014; Ko et al., 2014; Zhu et al., 2015).

At the protein interaction level, there are similarities as well as distinctions. MS23 interacts with bHLH51 but not bHLH122 (Fig. S14) paralleling its counterpart in rice (Fu et al., 2014; Ko et al., 2014). Additionally, MS32 only forms strong dimers with bHLH122 in maize whereas bHLH51 forms both homodimers and strong dimers with bHLH122. In *Arabidopsis*, interactions are less specific because all possible combinations tested positive among bHLH10, bHLH89, bHLH91, DYT1 and AMS (Xu et al., 2010; Feng et al., 2012). Neither the rice nor *Arabidopsis* anther proteomes has been investigated to determine which proteins are present simultaneously; however, we predict that bHLH partner exchange will be a common theme during anther development.

The timely deployment of various bHLH complexes regulates the sequential progression of TP into several distinctive roles over 2 weeks of anther development, ultimately leading to successful pollen production. MS23 is the earliest regulator identified, controlling a suite of TFs important for early TP development. It is present in the SPC at Stage 7 and continues to direct pre-tapetal cells into young TP at Stage 8. Because MS23 does not form homodimers, we hypothesize that during Stages 7 to 8, MS23 must form a heterodimer with an unknown factor (Fig. S17) to prevent periclinal divisions in pre-tapetal cells. By contrast, MS32 is not required until Stage 9 when excessive divisions are initially observed in the *ms32* mutant anthers. This timing of the *ms32* phenotype coincides with the first expression peak of bHLH122; therefore, the bHLH122-MS32 complexes are potentially the key for terminating periclinal divisions of TP beyond Stage 9. Next, at Stage 10, when *Ms23* is at its highest expression level and *bHLH51* expression reaches its first peak, the MS23-bHLH51 heterodimers might serve crucial roles for re-differentiation of the TP to nourish meiotic cells and accumulate materials utilized after meiosis. When bHLH122 transcripts reappear and *Ms23* levels off at Stage 11, we propose that bHLH51 breaks away from MS23 to bind with bHLH122 and also forms homodimers, both of which are likely to be essential for the next phase of TP development as secretory cells to dissolve tetrad callose and deposit exine onto pollen. There is support for this model in rice, in which competition between *TIP2* and *EAT1* has been suggested (Fu et al., 2014; Ko et al., 2014). Ultimately, we propose that bHLH51 homodimers initiate programmed cell death, as in rice and *Arabidopsis* (Zhang et al., 2008; Xu et al., 2010, 2014).

Each network in maize, rice and *Arabidopsis* is unique but includes the same protein types. We demonstrate that MS23 is the master factor during the 5-day period of tapetal specification and early differentiation in maize. MS32 has a more general role in multiple maize organs, and it is only indispensable at Stage 9 when it is required to slow further cell divisions and prevent periclinal divisions. In rice, a feedback relationship between *TIP2* and *UDT1* in parallel pathways is also proposed (Fu et al., 2014). A second report in rice, however, proposes a different hierarchy and puts *TIP2* downstream of *UDT1* (Ko et al., 2014), similar to the proposed network in *Arabidopsis*. Our maize data are more extensive in

capturing stage-specific events with more in-depth quantitative data analysis substantiated with proteomics, permitting clearer justification for the timing and deployment of bHLH complexes in the maize TP.

MATERIALS AND METHODS

Plant material

ms23-ref and *ms32* seeds were provided by Pat Bedinger (Colorado State University); *ms23-6027* and *ms23-6059* were obtained from the Maize Genetics COOP Stock Center (Urbana, IL, USA). Stocks were maintained by pollinating ears on male-sterile plants by pollen from a fertile, heterozygous sibling (*ms*×*F*) to maintain 1:1 segregating lines. To increase the visibility of recombination events in the mapping populations, *ms23-6027* and *ms23-6059* plants were introgressed once by crossing with B73 and A619 inbred lines followed by selfing (F1) then an *ms*×*F* cross (F2).

Map-based cloning

Total leaf genomic DNA was extracted from 23 male-sterile and 23 fertile sibling individuals in a 1:1 family for the *ms23-ref* allele. Each DNA sample was adjusted to 25 ng/μl before combining to make one sterile and one fertile pool for bulk segregation analysis at the Genomic Technologies Facility at Iowa State (Liu et al., 2010). PCR primers were tested to find polymorphic markers distinguishing fertile from sterile plants (Table S7). By scoring the presence/absence of recombinants at diverse marker locations, the interval containing the gene was narrowed to the tip of chromosome 8S and eventually to gene model GRMZM2G021276.

Phylogenetic analysis

Protein sequences of the putative orthologs of MS23 were obtained from Gramene (<http://www.gramene.org>) and aligned using Cobalt (<http://www.st-vancouver.nlm.nih.gov/tools/cobalt/cobalt.cgi?CMD=Web>). A maximum likelihood tree using a Poisson model with the highest likelihood was generated using MEGA 6.06 (Tamura et al., 2013; <http://www.megasoftware.net/>).

RNA extraction, microarray hybridization, qRT-PCR, *in situ* RNA hybridization and RNA-seq

Various organs, including anthers, were collected directly into tubes chilled in liquid nitrogen. Total maize RNA was isolated using the PureLink RNA Mini Kit (Invitrogen) incorporating TRIzol Reagent (Invitrogen) with an on-column DNase I (Qiagen) digestion according to the manufacturer's instructions. Microarray experiments were conducted as previously described (Nan et al., 2011). qRT-PCR was performed as previously described with three biological samples and three technical replicates unless stated otherwise (Zhang et al., 2014). Table S8 lists the PCR primer sequences used in this study. For *in situ* hybridization, immature 3–5 cm tassels were fixed and embedded in paraffin following a standard protocol (Jackson et al., 1994). Sections (7 μm) were hybridized as previously described (Zhang et al., 2014) using probes synthesized from PCR-generated fragments with 5'-ATTTAGGTGACACTATAGAAGAGCGATCCGAGCACGTACA-3' and 5'-TAATACGACTCACTATAGGGAGAACCCTTGTGAATCTTGGTG-3' primer pairs.

RNA-seq libraries were constructed using TruSeq RNA Sample Prep kits (Illumina). PARE libraries were constructed as previously described (Zhai et al., 2014). All libraries were sequenced on an Illumina HiSeq 2500 instrument at the Delaware Biotechnology Institute.

Confocal microscopy

Anthers were collected directly into 100% ethanol and stored at 4°C until staining and imaging utilizing protocols described previously (Kelliher and Walbot, 2011).

Yeast two-hybrid assay

The bHLH domains of MS23, MS32, bHLH122 and bHLH51 were PCR amplified (Table S9) and cloned into pCR2.1-TOPO vectors (Invitrogen). Clones with correct, in-frame sequences were subcloned into both the bait (pGBKT7) and/or prey (pGADT7) vectors (Clontech). Co-transformation

bait and prey vectors into competent AH109 yeast cells (*MATa, trp1-901, leu2-3, 112, ura3-52, his3-200, gal4Δ, gal80Δ, LYS2* :: GAL1_{UAS}-GAL1_{TATA}-HIS3, GAL2_{UAS}-GAL2_{TATA}-ADE2, URA3 :: MEL1_{UAS}-MEL1_{TATA}-lacZ) was performed using a modified lithium acetate-mediated method (Clontech). Yeast clones containing both a bait and a prey were selected on low stringency SD plate (SD/-Leu/-Trp; Clontech). Interactions were further verified by screening on high stringency SD plates (SD/-Ade/-His/-Leu/-Trp; Clontech).

Proteomics

Fertile anthers from the W23 inbred were used. Approximately 300 anthers at 1000 μm and 100 anthers at 2000 μm were collected directly into 1.5-ml screw-cap tubes chilled in liquid nitrogen. Pollen was collected from an actively shedding tassel and immediately stored in liquid nitrogen. Trypsin-digested protein samples were analyzed by HPLC-MS/MS as described by Facette et al. (2013) using duplicate samples.

Acknowledgements

We thank K. van der Linde for advice on yeast two-hybrid assays; M.R. Facette of University of California at San Diego for assistance with the proteomic data analysis; H. Cartwright for assistance with the use of confocal microscope at the Carnegie Institution for Science - Department of Plant Biology; and members of the Walbot laboratory for valuable discussions and comments on the manuscript.

Competing interests

The authors declare no competing or financial interests.

Author contributions

G.-L.N. and V.W. conceived and designed the experiments; G.-L.N. conducted the research; J.Z. analyzed the RNA-seq data; S.A. generated the RNA-seq libraries; D.M., L.M. and N.N. performed the microarray experiments; J.F. analyzed the array data; G.-L.N., B.C.M. and V.W. wrote the manuscript; all authors read and approved the manuscript.

Funding

This work was supported by a National Science Foundation IOS award (#1339229).

Data availability

Microarray and RNA-seq data have been deposited in <http://www.ncbi.nlm.gov/geo> under accession numbers GSE90968 and GSE90849, respectively.

Supplementary information

Supplementary information available online at <http://dev.biologists.org/lookup/doi/10.1242/dev.140673.supplemental>

References

- Carretero-Paulet, L., Galstyan, A., Roig-Villanova, I., Martínez-García, J. F., Bilbao-Castro, J. R. and Robertson, D. L. (2010). Genome-wide classification and evolutionary analysis of the bHLH family of transcription factors in *Arabidopsis*, Poplar, Rice, Moss, and Algae. *Plant Physiol.* **153**, 1398-1412.
- Chaubal, R., Zanella, C., Trimmell, M. R., Fox, T. W., Albertsen, M. C. and Bedinger, P. (2000). Two male-sterile mutants of *Zea mays* (Poaceae) with an extra cell division in the anther wall. *Am. J. Bot.* **87**, 1193-1201.
- Chaubal, R., Anderson, J. R., Trimmell, M. R., Fox, T. W., Albertsen, M. C. and Bedinger, P. (2003). The transformation of anthers in the *msc1* mutant of maize. *Planta* **216**, 778-788.
- Egger, R. L. and Walbot, V. (2016). A framework for evaluating developmental defects at the cellular level: An example from ten maize anther mutants using morphological and molecular data. *Dev. Biol.* **419**, 26-40.
- Facette, M. R., Shen, Z., Fjola, R., Björnsdóttir, F. R., Briggs, S. P. and Smith, L. G. (2013). Parallel proteomic and phosphoproteomic analyses of successive stages of maize leaf development. *Plant Cell* **25**, 2798-2812.
- Feng, B., Lu, D., Ma, X., Peng, Y., Sun, Y., Ning, G. and Ma, H. (2012). Regulation of the *Arabidopsis* anther transcriptome by DYT1 for pollen development. *Plant J.* **72**, 612-624.
- Fu, Z., Yu, J., Cheng, X., Zong, X., Xu, J., Chen, M., Li, Z., Zhang, D. and Liang, W. (2014). The rice Basic Helix-Loop-Helix transcription factor TDR INTERACTING PROTEIN2 is a central switch in early anther development. *Plant Cell* **26**, 1512-1524.
- Jackson, D., Veit, B. and Hake, S. (1994). Expression of maize KNOTTED1 related homeobox genes in the shoot apical meristem predicts patterns of morphogenesis in the vegetative shoot. *Development* **120**, 405-413.
- Ji, C., Li, H., Chen, L., Xie, M., Wang, F., Chen, Y. and Liu, Y.-G. (2013). A novel rice bHLH transcription factor, DTD, acts coordinately with TDR in controlling tapetum function and pollen development. *Mol. Plant* **6**, 1715-1718.
- Jung, K. H., Han, M. J., Lee, Y. S., Kim, Y. W., Hwang, I., Kim, M. J., Kim, Y. K., Nahm, B. H. and An, G. (2005). Rice *Undeveloped Tapetum1* is a major regulator of early tapetum development. *Plant Cell* **17**, 2705-2722.
- Kelliher, T. and Walbot, V. (2011). Emergence and patterning of the five cell types of the *Zea mays* anther locule. *Dev. Biol.* **350**, 32-49.
- Kelliher, T., Egger, R. L., Zhang, H. and Walbot, V. (2014). Unresolved issues in pre-meiotic anther development. *Front. Plant Sci.* **5**, 347.
- Ko, S.-S., Li, M.-J., Ku, M. S.-B., Ho, Y.-C., Lin, Y.-J., Chuang, M.-H., Hsing, H.-X., Lien, Y.-C., Yang, H.-T., Chang, H.-C. et al. (2014). The bHLH142 transcription factor coordinates with TDR1 to modulate the expression of EAT1 and regulate pollen development in rice. *Plant Cell* **26**, 2486-2504.
- Li, N., Zhang, D.-S., Liu, H.-S., Yin, C.-S., Li, X.-X., Liang, W.-Q., Yuan, Z., Xu, B., Chu, H.-W., Wang, J. et al. (2006). The rice *Tapetum Degeneration Retardation* gene is required for tapetum degradation and anther development. *Plant Cell* **18**, 2999-3014.
- Lin, J.-J., Yu, C.-P., Chang, Y.-M., Chen, S. C.-C. and Li, W.-H. (2014). Maize and millet transcription factors annotated using comparative genomic and transcriptomic data. *BMC Genomics* **15**, 818.
- Liu, S., Chen, H. D., Makarevitch, I., Shirner, R., Emrich, S. J., Dietrich, C. R., Barbazuk, W. B., Springer, N. M. and Schnable, P. S. (2010). High-throughput genetic mapping of mutants via quantitative single nucleotide polymorphism typing. *Genetics* **184**, 19-26.
- Ma, J., Duncan, D., Morrow, D. J., Fernandes, J. and Walbot, V. (2007). Transcriptome profiling of maize anthers using genetic ablation to analyze pre-meiotic and tapetal cell types. *Plant J.* **50**, 637-648.
- Moon, J., Skibbe, D., Timofejeva, L., Wang, C.-J. R., Kelliher, T., Kremling, K., Walbot, V. and Cande, W. Z. (2013). Regulation of cell divisions and differentiation by MALE STERILITY32 is required for anther development in maize. *Plant J.* **76**, 592-602.
- Nan, G.-L., Ronceret, A., Wang, R. C., Fernandes, J. F., Cande, W. Z. and Walbot, V. (2011). Global transcriptome analysis of two *ameiotic1* alleles in maize anthers: defining steps in meiotic entry and progression through prophase I. *BMC Plant Biol.* **11**, 120.
- Nguyen Ba, A. N., Pogoutse, A., Provart, N. and Moses, A. M. (2009). NLStradamus: a simple Hidden Markov Model for nuclear localization signal prediction. *BMC Bioinformatics* **10**, 202.
- Niu, N., Liang, W., Yang, X., Jin, W., Wilson, Z. A., Hu, J. and Zhang, D. (2013). EAT1 promotes tapetal cell death by regulating aspartic proteases during male reproductive development in rice. *Nat. Commun.* **4**, 1445.
- Sanders, P. M., Bui, A. Q., Weterings, K., McIntire, K. N., Hsu, Y.-C., Lee, P. Y., Truong, M. T., Beals, T. P. and Goldberg, R. B. (1999). Anther developmental defects in *Arabidopsis thaliana* male-sterile mutants. *Sex. Plant Reprod.* **11**, 297-322.
- Skibbe, D. S. and Schnable, P. S. (2005). Male sterility in maize. *Maydica* **50**, 367-376.
- Sorensen, A.-M., Kröber, S., Unte, U. S., Huijser, P., Dekker, K. and Saedler, H. (2003). The *Arabidopsis* ABORTED MICROSPORES (AMS) gene encodes a MYC class transcription factor. *Plant J.* **33**, 413-423.
- Tamura, K., Stecher, G., Peterson, D., Filipowski, A. and Kumar, S. (2013). MEGA6: molecular evolutionary genetics analysis version 6.0. *Mol. Biol. Evol.* **30**, 2725-2729.
- Timofejeva, L., Skibbe, D. S., Lee, S., Golubovskaya, I., Wang, R., Harper, L., Walbot, V. and Cande, W. Z. (2013). Cytological characterization and allelism testing of anther developmental mutants identified in a screen of maize male sterile lines. *Genes Genomes Genetics* **3**, 231-249.
- Tsou, C.-H., Cheng, P.-C., Tseng, C.-M., Yen, H.-J., Fu, Y.-L., You, T.-R. and Walden, D. B. (2015). Anther development of maize (*Zea mays*) and longstamen rice (*Oryza longistaminata*) revealed by cryo-SEM, with foci on locular dehydration and pollen arrangement. *Plant Reprod.* **28**, 47-60.
- Vernoud, V., Laigle, G., Rozier, F., Meeley, R. B., Perez, P. and Rogowsky, P. M. (2009). The HD-ZIP IV transcription factor OCL4 is necessary for trichome patterning and anther development in maize. *Plant J.* **59**, 883-894.
- Wang, C.-J. R., Nan, G.-L., Kelliher, T., Timofejeva, L., Vernoud, V., Golubovskaya, I. N., Harper, L., Egger, R., Walbot, V. and Cande, W. Z. (2012). Maize *multiple archesporial cells 1 (mac1)*, an ortholog of rice *TDL1A*, modulates cell proliferation and identity in early anther development. *Development* **139**, 2594-2603.
- Xu, J., Yang, C., Yuan, Z., Zhang, D., Gondwe, M. Y., Ding, Z., Liang, W., Zhang, D. B. and Wilson, Z. A. (2010). The ABORTED MICROSPORES regulatory network is required for postmeiotic male reproductive development in *Arabidopsis thaliana*. *Plant Cell* **22**, 91-107.
- Xu, J., Ding, Z., Vizcay-Barrena, G., Shi, J., Liang, W., Yuan, Z., Werck-Reichhart, D., Schreiber, L., Wilson, Z. A. and Zhang, D. (2014). ABORTED MICROSPORES acts as a master regulator of pollen wall formation in *Arabidopsis*. *Plant Cell* **26**, 1544-1556.
- Zhai, J., Arikait, S., Simon, S. A., Kingham, B. F. and Meyers, B. C. (2014). Rapid construction of parallel analysis of RNA end (PARE) libraries for Illumina sequencing. *Methods* **67**, 84-90.
- Zhai, J., Zhang, H., Arikait, S., Huang, K., Nan, G.-L., Walbot, V. and Meyers, B. C. (2015). Spatiotemporally dynamic, cell-type dependent pre-meiotic and meiotic phasiRNAs in maize anthers. *Proc. Natl. Acad. Sci. USA* **112**, 3146-3151.
- Zhang, D. and Wilson, Z. A. (2009). Stamen specification and anther development in rice. *Chin. Sci. Bull.* **54**, 2342-2353.

- Zhang, W., Sun, Y., Timofejeva, L., Chen, C., Grossniklaus, U. and Ma, H.** (2006). Regulation of Arabidopsis tapetum development and function by *DYSFUNCTIONAL TAPETUM1 (DYT1)* encoding a putative bHLH transcription factor. *Development* **133**, 3085-3095.
- Zhang, D.-S., Liang, W.-Q., Yuan, Z., Li, N., Shi, J., Wang, J., Liu, Y.-M., Yu, W.-J. and Zhang, D.-B.** (2008). *Tapetum Degeneration Retardation* is critical for aliphatic metabolism and gene regulation during rice pollen development. *Mol. Plant* **1**, 599-610.
- Zhang, H., Egger, R. L., Kelliher, T., Morrow, D., Fernandes, J., Nan, G.-L. and Walbot, V.** (2014). Transcriptomes and proteomes define gene expression progression in pre-meiotic maize anthers. *Genes Genomes Genetics* **3**, 993-1010.
- Zhu, E., You, C., Wang, S., Cui, J., Niu, B., Wang, Y., Qi, J., Ma, H. and Chang, F.** (2015). The DYT1-interacting proteins bHLH010, bHLH089 and bHLH091 are redundantly required for Arabidopsis anther development and transcriptome. *Plant J.* **83**, 976-990.

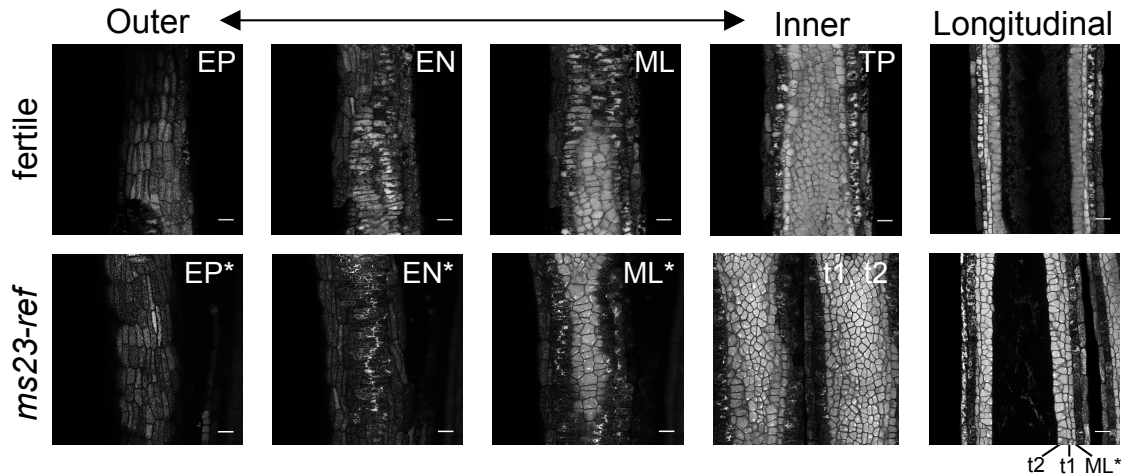


Fig. S1. Confocal images of the *ms23-ref* and its fertile sibling anthers at various depths (Z-axis) at Stage 10. The cell shape and morphology of EP versus EP*, EN versus EN, and ML versus ML* are indistinguishable at this stage. The two innermost layers (t1 and t2) in mutant anther are indistinguishable from each other under confocal from the XY-planes, indicating these two layers are sisters resulting from extra periclinal divisions while ML* is formed earlier. Judging from the central, longitudinal plane, however, t1 cells have a shorter Z-dimension, similar to ML/ML*, while t2 cells have a longer Z-dimension, resembling TP. In fertile anthers, EP – epidermis; EN – endothecium; ML – middle layer; TP – tapetum. In *ms23-ref* anthers, EP* - the presumptive epidermis; EN* - the presumptive endothecium; ML* - the presumptive middle layer; t1 – the defective fourth layer; t2 – the defective fifth layer.

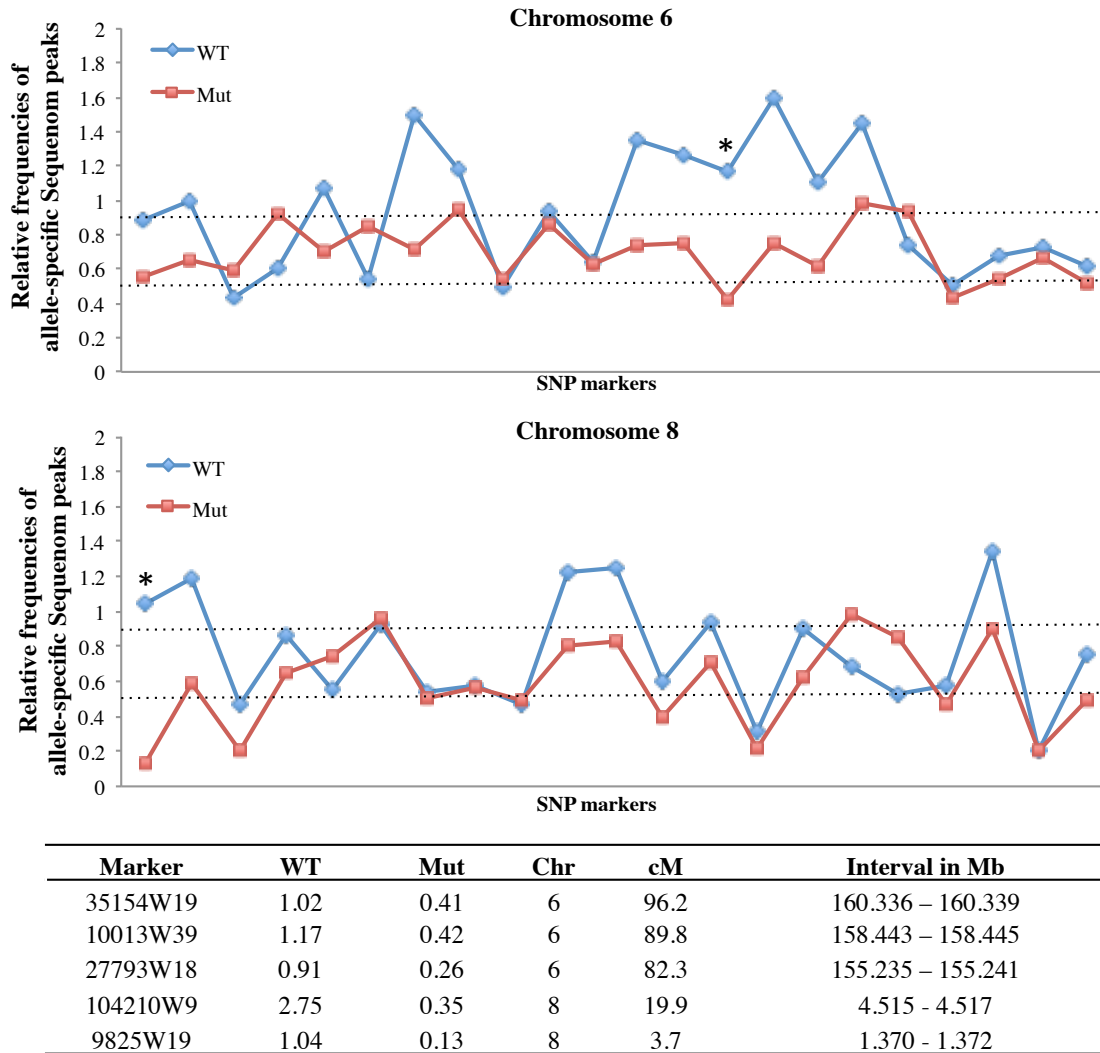


Fig. S2. High-throughput genetic mapping of *Ms23* via quantitative SNP-genotyping on a Sequenom chip. Segregating *ms23-ref* mutant (Mut) and wildtype (WT) genomic DNA pools were analyzed using the Maize Bulk Segregation Analysis service at the Genomic Technologies Facility at Iowa State University against a set of SNP markers (n=1,016). Using 0.9 and 0.5 cut-offs for wildtype (WT) and mutant (Mut) pools, respectively, *Ms23* was placed on chromosomes 6 and 8 at the locations indicated (*).

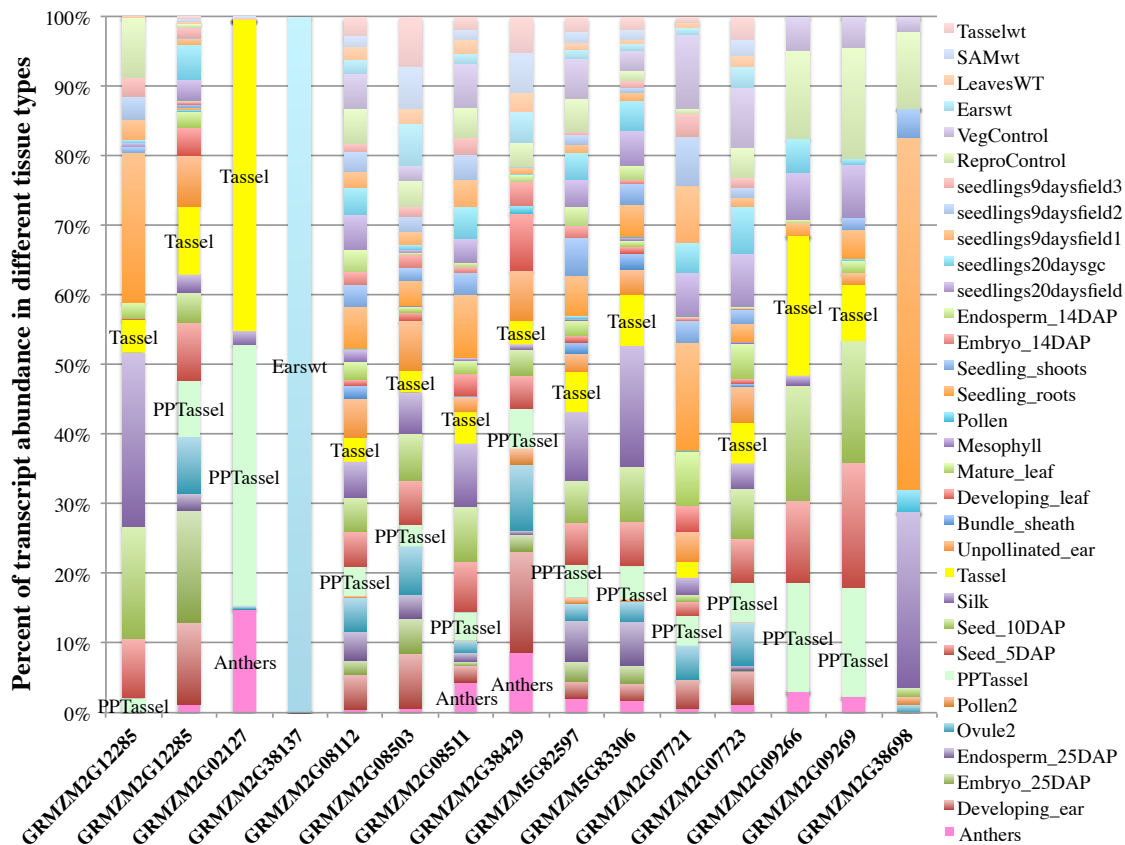
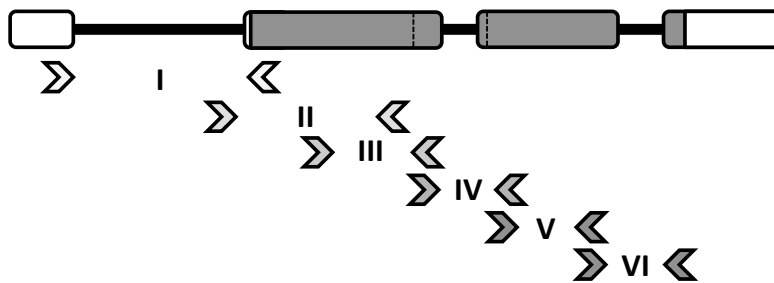


Fig. S3. Tissue-specific transcript abundances of fifteen gene models near the tip of chromosome 8 based on the data on qTeller (<http://qteller.com/>). Y-axis is the percentage of transcript abundance in each tissue type over the sum of abundance from all 32 tissues as 100%.

A

GTTTAATAACCTTGCCTGCGCAGTAGCCCTTAACTGCTGCTATCTATCTCTTTTCTGAAGGAAAAAAAA
 GGTGGTACTCTCTACTAGCTAGTCCCTGCATGCCGCTAATGTGCGTCTTGCCCTGTTTATTTGTTCTTA
 ATAAGGGCTGCCTATCTATTATATTTTTGCACCTGTTTTGCTGTGTTCTTGGTAACTAGCTTAATTCCTTCG
 CCTACAATCGTCAAATCCCCCATCATCAGTCAGATGAACCTTTGATCGAATTGAAGTTGTTCTTCTAAT
 TCGGCCCCAGCAGCCCATGCATCTGGTTTTATTGCTTTCTGTTGGGTATAATATGCAAGACCTTTTGT
 TGCTAGGGCAAGGCTGCAACCACATGCGTGTACTGAACCTCATGATGTAACCTCATCTTTTTGTTGCTCAC
 AGAATCACTACTCTACTGCACCTTCTTTTCATCCGATCCGCAATCTTTTTTTTTCTTTTACATGCTTTAGTT
 TTCTCTCTTTCTTGATTACAAACATGATTACTGGAACCTTTCTTAGGCTGCCTTCCCCTTCTTGGATCTGC
 TTTAGTTTTCTTTTTTGGGCTACCGCGCGCGGCTTATTTGAGTTTATCACTTGCATATACATAATATA
 TATATACATGCATGCGATGGCGTTCATGTTACTCAACTACAGATCTGTTTCTGTTCTGTTGTTTTCAGTTCA
 CGCGCAGTTAAGCATAGCAGGACGACCAGCAGCATACCCGAGTGCAGCTC CTGACGATGGCG
 CACGAAACGCCGACCTGGACGCCGCGCCAGCCACCTAACCGTCTCCGGCGTCGCCAGCATCCCGGCA
 GCTGAGCTTCCACCTGCTGCACTCGCTCGACGCCGCGGCGGGTCAATCCCCTCACGGCGCCGCCGAGT
 CCACCATCGACTACTTCCCTCGGCGCGCCGATCCCCACCAGCAGGCCATGCAGTACGAGCCGCTGCCGCC
 GCCGCGGGCGGCCACCACCAGTACACCATGGACATGTTCCGCGACTACTGCGACGCCACTACCCACCGC
 CGAGCCGTACATCCGCGGGACAATGACTGGAGCCCTCGTGTTCGGGGCCACCAGCAGCAGACTCGGCCG
 CTGCCCTACAT GCGCGGGGGCACTTTGAGACCTCCCCGCGCCGCCACGCGCCACCGGCCGCGGCAGGAA
 CGGGGACAGGCGCTGGGCGCGGCTTCCATGCTGTGCTGGCAACGGCGTCGAGAAGAAGGAGAAGCAGC
 GCGCGCTGCGGGCTACCCGAGAAGTACACCGCCCTCATGCACTCATAACCAACGTTACAAAGGTCGTACCA
 AATCTCCTCTTATGTTTCGTCATCGTTTCAAATTAAGTTAAAAAATTAATTCACGGTCTTGTGTTTAT
 TTTTTGCGCACTGCAG ACTGATAGGGCGACGGTGTCTCGGACGGATCGAGTACATCCAGGAGCTGGGGA
 GGACGGTGGAGGAGCTGACGCTGCTGGTGGAGAAGAAGCGGCGCCGGAGGGAGCTGCAGGGGACGTCGTG
 GACGCGGCGCGGCTGCGGTGGTTGCTGCCCGGCTGAGGCGGAGAGCTCGGAGGGCGAGGTGGCTCCTCC
 GCCGCGGGCGTGCCTGCGGCGCAGCCGATCCGGAGCAGTACATCCAGCGGGGAGCAAGGACACGTCCTGTTG
 ACGTGGGATCGTGGAGGAGGACGTGAACATCAAGCTACCAAGCCGGCGCGACGGGTGCCCTGCAGCC
 GCGTCGCGCGCTGGATGACCTCCGCTTACCTCGTCCACCTCTCCGGCGCAAGATCGGTGACTGTCA
 AATCTACATGTTCAACACCAAGGTACATACGAATACGATACGTAGCCATTGATCGATCTGTAATTCGTAG
 CCTGACGATTCCGAGGTTTCTGGTGTAAAAATGCATCTTTTTTCTCAGATGACAATGCTTTCTGTCTT
 TGTTACCCGAGATTCACAAGGGGTCTTCAGTGTTCGAGTGCAGTGGCCGGTAGGCTGATGGAAGTGGT
 GGACGAGTACTAGGCTACCATGCACCTGAATTTCTAGCTAGCTCTACGTACCCGCTGCTATGAATCTAGC
 TATAGCTTTCTTGGATGAAAGACTAGTTAGTTGTTACCTTCTATCTTTGCTTCAATTAATCCGCTTGTCT
 CGTTACAGACTGATTTTCTTAAATGTCAAGGTTGTTTTGGTCAAATTAATTAATTAATTAATTAATTAAT
 TGTGAGGTTATTATATATATTTATGTGTTTATTACTGGTCTATTAATTTGTCTTATTATTA

B

	Forward Primer	Reverse Primer
I	TGCACCTGTTTTGCTGTGTT	TGATACATCGTCTGGTCTGT
II	CGACCACGACGATGTATCAC	CGCTGCTTCTCCTTCTTCTC
III	ACTACTGCGACGGCCACTAC	CATGAGGGCGGTGTACTTCT
IV	CGGCTCACCGAGAAGTACAC	CCGCTTCTTCTCCACCAG
V	GAGGAGCTGACGCTGCTG	CCGCTTCTTCTCCACCAG
VI	GTGGAGGAGGACGTGAACAT	ACTCGTCCACCCTTCCATC

Fig. S4. Cloning of *Ms23*. (A) The nucleotide sequence of GRMZM2G021276 with the four exons underlined, the translated region in bold, and the encoded bHLH domain in blue. The positions of frameshift mutations in the *ms23-6027* and *ms23-6059* alleles are indicated as orange and green arrows, respectively. (B) Placement and sequences of the PCR primers across the gene model of *bHLH16* (GRMZM2G021276).

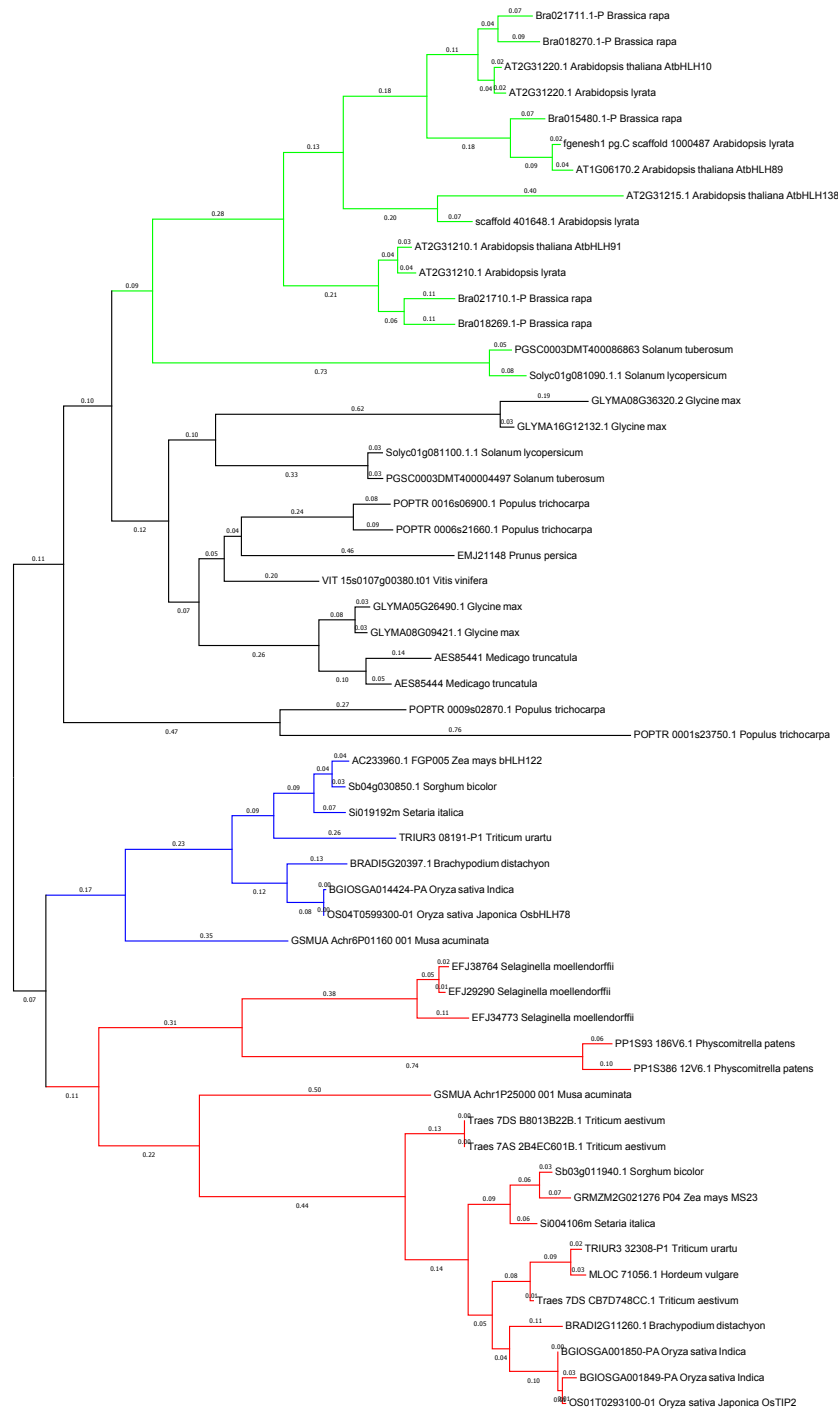


Fig. S5. Phylogenetic analysis of the orthologs of both MS23 and its paralog, bHLH122, (<http://www.gramene.org/>). The tree was generated using MEGA 6.06 (Tamura et al., 2013) by the maximum likelihood method based on the Poisson model; the tree with the highest log likelihood (-29072.8504) is shown. The tree is drawn to scale, with branch lengths measured in the number of substitutions per site. The analysis involved 55 amino acid sequences. There were a total of 1,146 positions in the final dataset.

Gene	Species	[BASIC] [HELIX] ~ LOOP ~ [HELIX]	No. of amino acids
MS23	<i>Zea mays</i>	ANGVEKKEKQRRRLRTEKYTALMHLIPNVTKTDRATVISDAIEYIQELGRVVEELTLV	59
TIP2/bHLH142	<i>Oryza sativa</i>	ANGVEKKEKQRRRLRTEKYNALMLLIPNRTKEDRATVISDAIEYIQELGRVVEELTLV	59
bHLH89	<i>Arabidopsis thaliana</i>	KRKIFPTEERRRVHFKDRFGDLKNLIPNPTKNDRASIVGEAIDYIKELLRTIDEFKLLV	59
bHLH10	<i>Arabidopsis thaliana</i>	KSRTSPTERRRVHFNDRFFDLKNLIPNPTKIDRASIVGEAIDYIKELLRTIEEFKMLV	59
bHLH91	<i>Arabidopsis thaliana</i>	KNKPFTEERRRCHLNERYEALKLLIPSPSKGDRASILQDGIDYINELRRRVSELKYL	59
bHLH122	<i>Zea mays</i>	KAN-FATERERREQFNVKYGALRSLFPNPTKNDRASIVGEAIDYINELNRTVKELKILL	58
EAT1/DTD	<i>Oryza sativa</i>	KAN-FATERERREQLNVKFRTLRMLFPNPTKNDRASIVGEAIDYIDELNRTVKELKILL	58
bHLH51	<i>Zea mays</i>	QCKNLEAERKRRKLNERYKLRSLVPNISKMDRAAILGDAIDYIVGLQNVKALQDEL	59
TDR	<i>Oryza sativa</i>	QCKNLEAERKRRKLNGLHYKLRSLVPNITKMDRASILGDAIDYIVGLQKQVKELQDEL	59
AMS	<i>Arabidopsis thaliana</i>	QAKNLEAERKRRKLNDRLYALRSLVPNITKMDRASILGDAINYVKELQNEAKELQDEL	59
MS32	<i>Zea mays</i>	KSKNLEAERKRRGKLNRRNIALRAVVPNITKMSKESTLSDAIDLKRLQNVLELQRQL	59
UDT1	<i>Oryza sativa</i>	KSKNLEAERRRRGRLNGNIFALRAVVPKITKMSKEATLSDAIEHIKNLQNEVLELQRQL	59
DYT1	<i>Arabidopsis thaliana</i>	KSPNLEAERRRRREKLHCLRLMALRSHVPIVTNMTKASIVEDAITYIGELQNNVKNLLET	59

:.: : : * . * : : : . : : : * : .

Fig. S6. Multiple sequence alignment of the bHLH domains of fourteen tapetum-associated bHLH proteins from maize, rice, and Arabidopsis. A partially duplicated pseudogene, *bHLH138* from Arabidopsis is excluded. An asterisk (*) indicates positions that have an invariant residue; a column (:) indicates conservation between groups of strongly similar properties with scoring > 0.5 in the Gonnet PAM 250 matrix; a period (.) indicates conservation between groups of weakly similar properties with scoring ≤ 0.5.

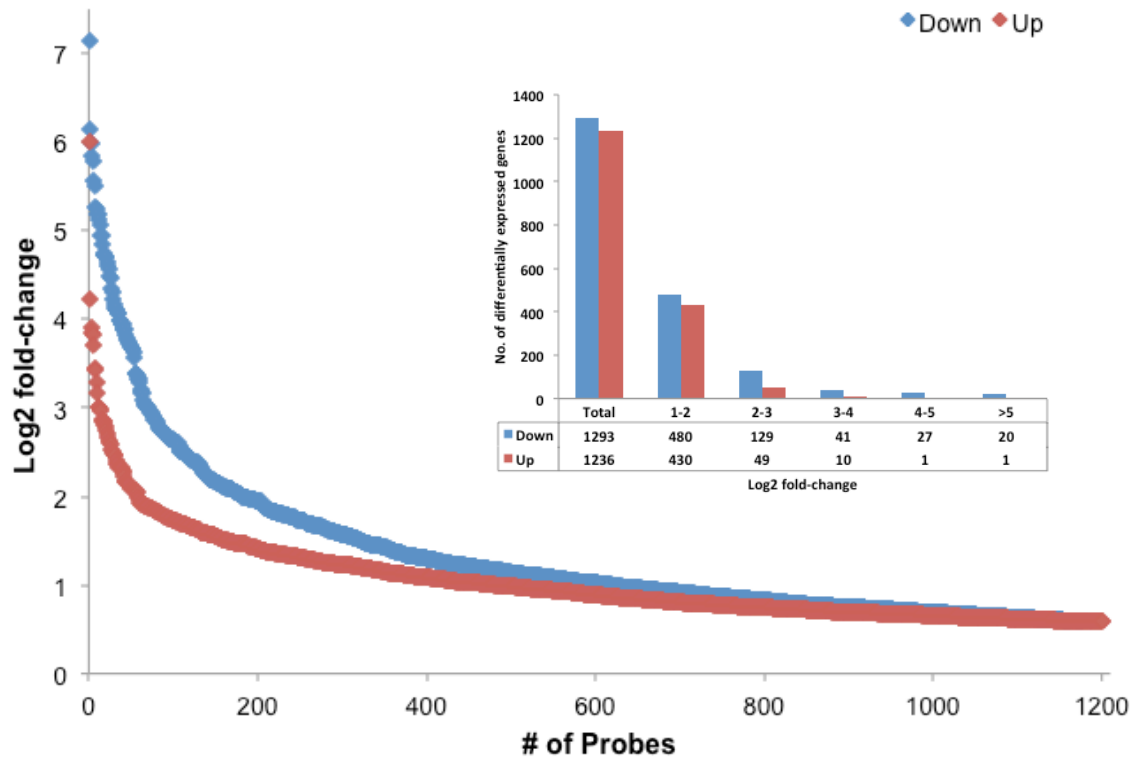


Fig. S7. Distribution of differentially expressed genes in *ms23-ref* mutant on the array. Up- and down-regulated genes comparing *ms23-ref* to its fertile sibling at Stage 9 were plotted based on their \log_2 fold change values. Inset: Counts of genes at different ranges of fold changes.

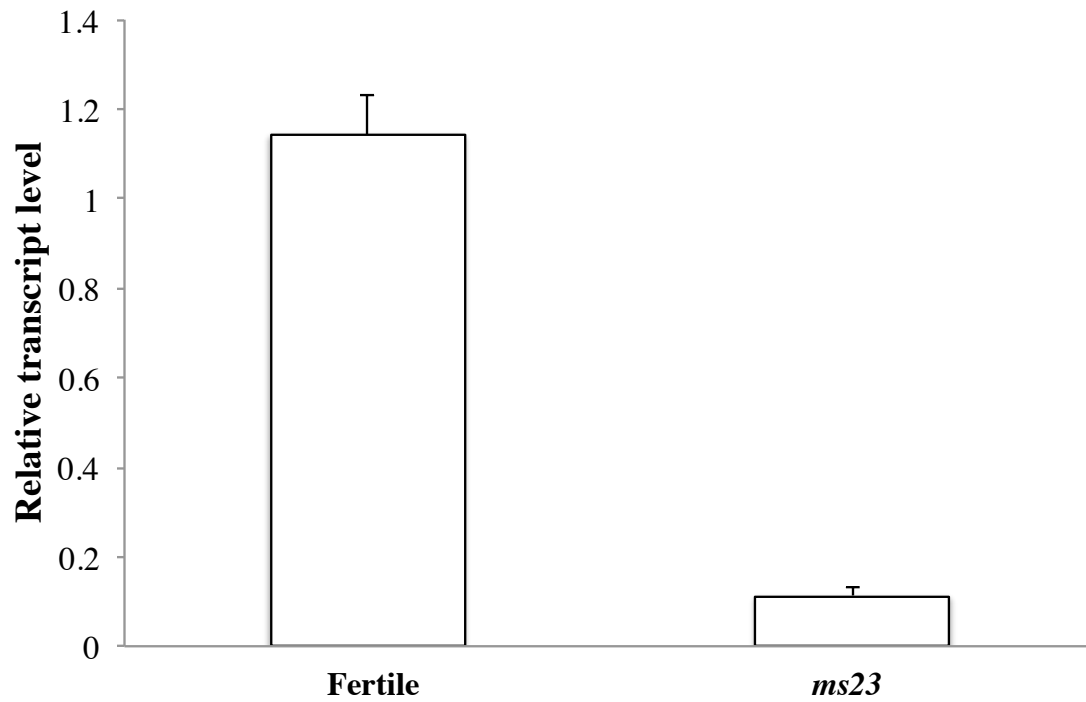


Fig. S8. Quantitative RT-PCR assays of *Dcl5* expression. *Dcl5* transcript levels in fertile and *ms23-ref* anthers at Stage 8. Expression values were normalized to the cyanase gene.

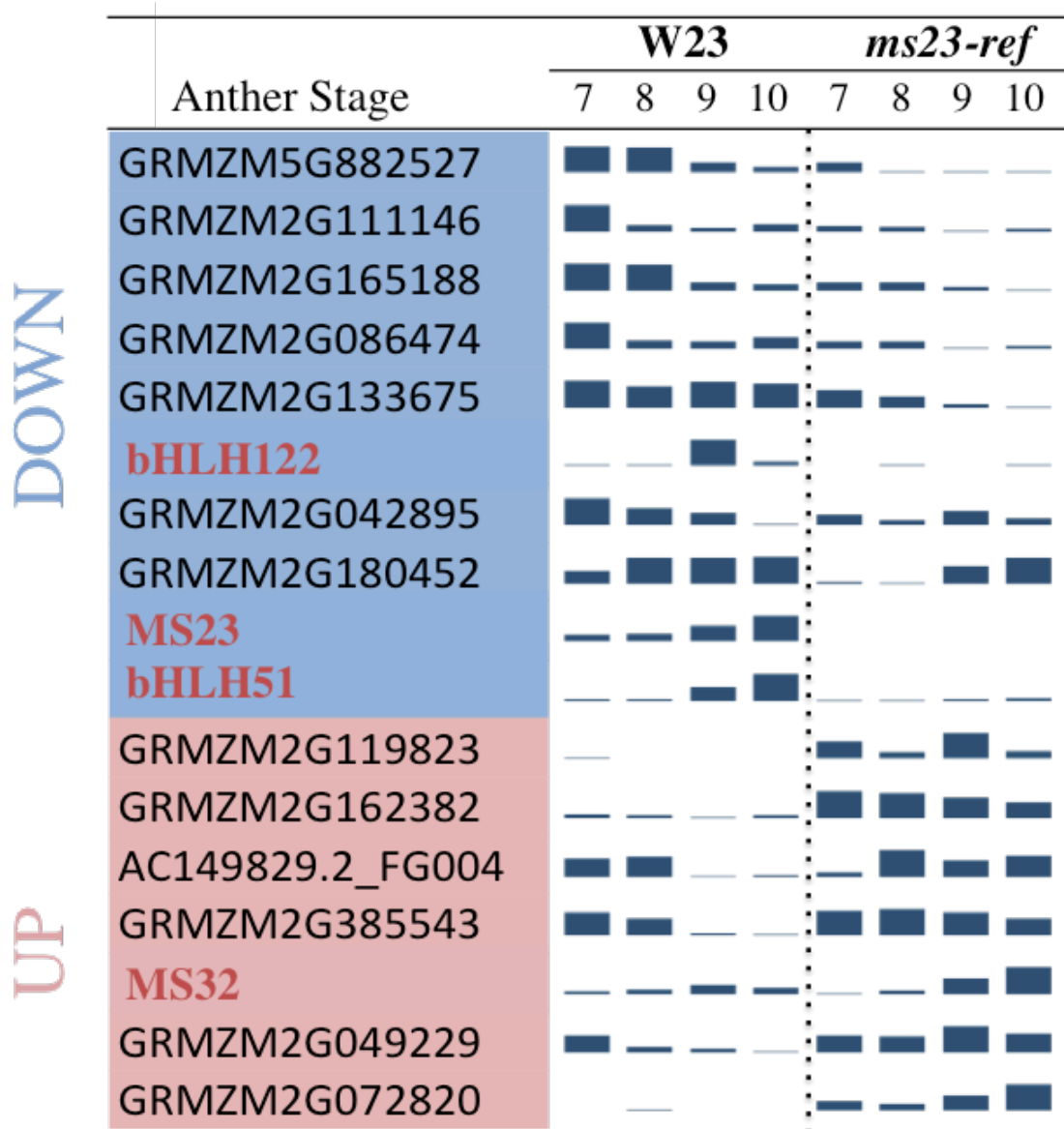


Fig. S9. Role of *Ms23* in regulating expression of the bHLHs with highest transcript abundance in fertile anthers. Maize bHLH genes with the sum of abundance in the top quartile (n=75) and with 4-fold or more difference (n=18) between *ms23-ref* mutant and W23 fertile anthers. Data are from RNA-seq analysis.

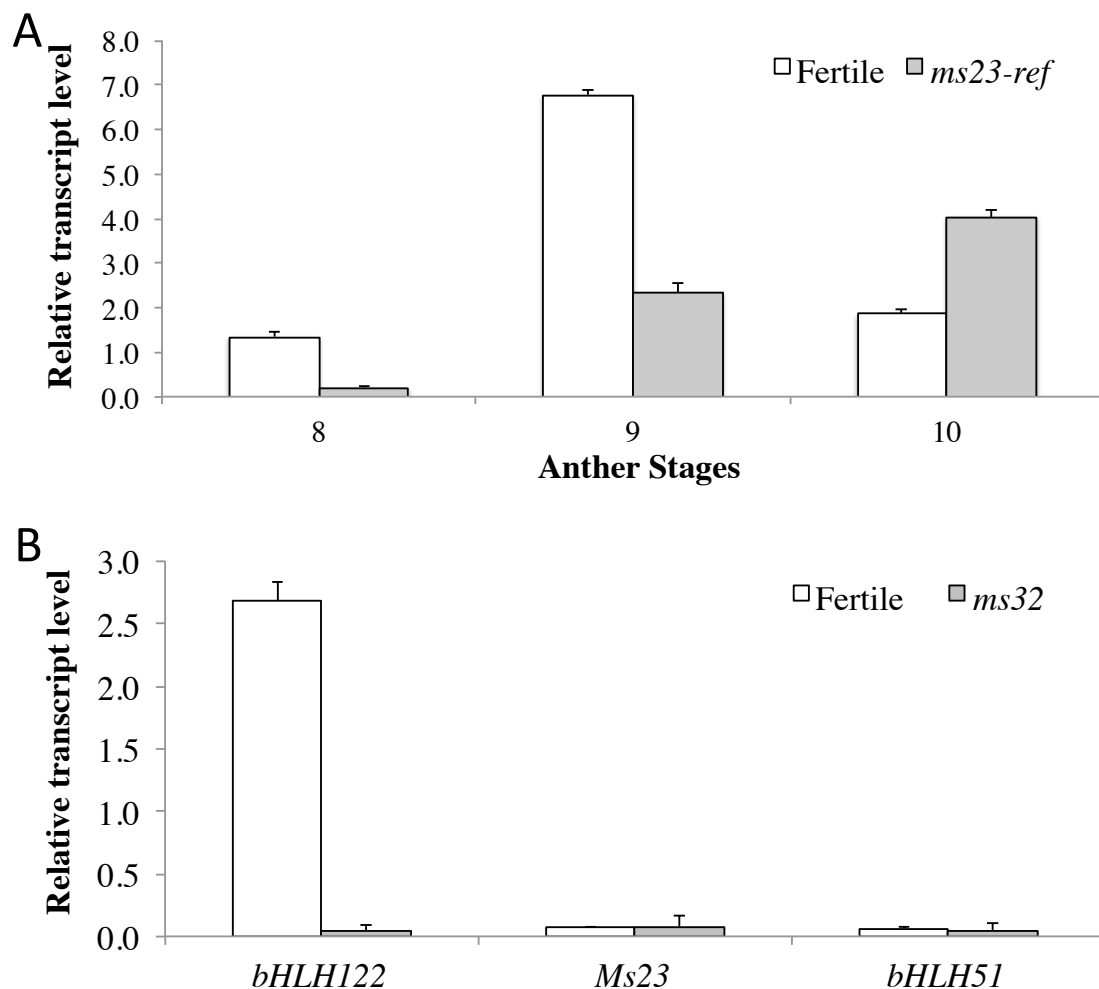


Fig. S10. Quantitative RT-PCR assays of gene expression. (A) *Ms32* transcript levels in fertile and *ms23-ref* anthers at various anther stages. (B) *Ms23*, *bHLH122*, and *bHLH51* transcript levels in fertile and *ms32* anthers at Stage 9. Expression values were normalized to the cyanase gene.

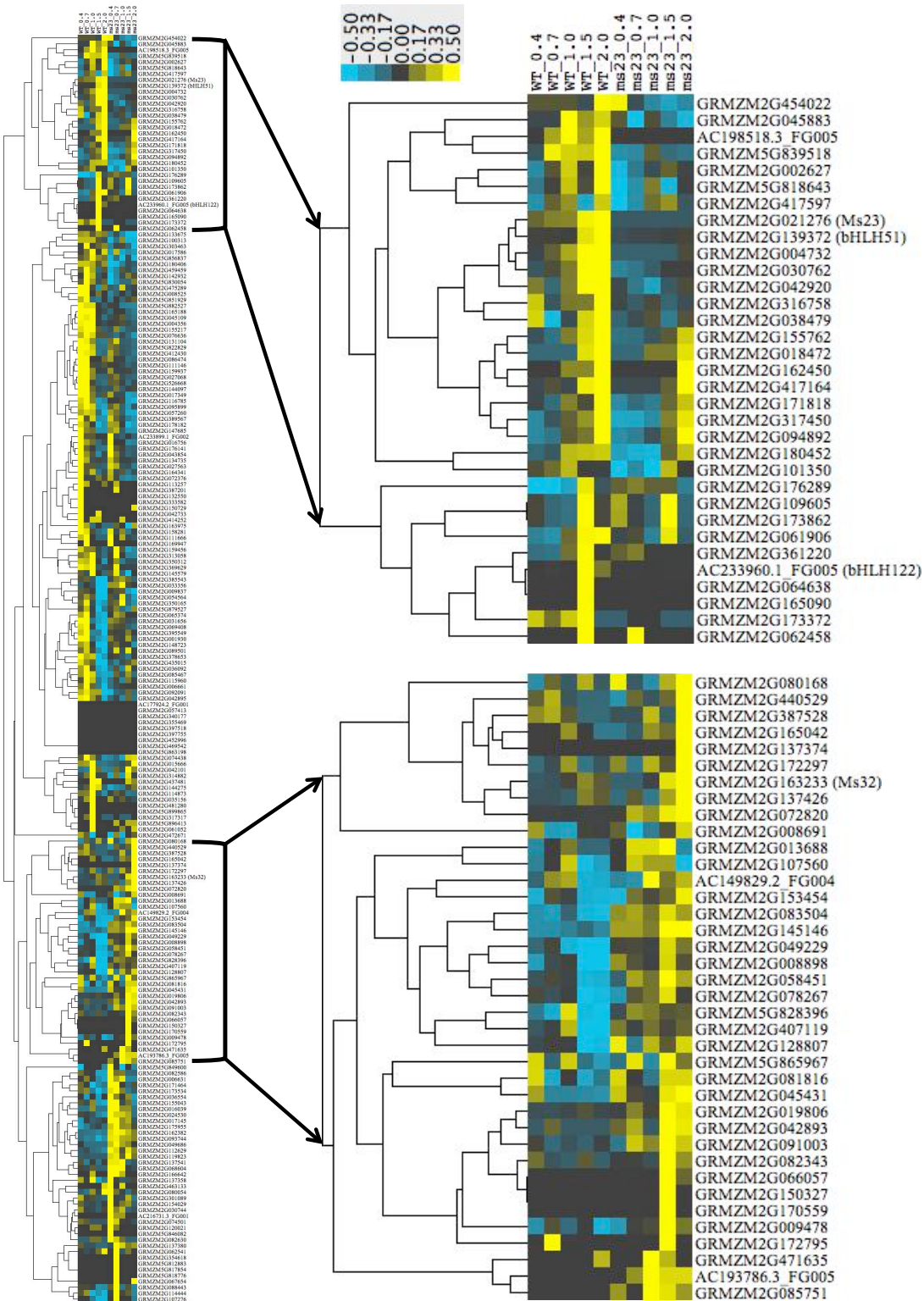


Fig. S11. K-median clustering of 213 maize bHLHs based on the expression patterns in both W23 fertile and *ms23-ref* anthers at stages 4, 7, 8, 9, and 10. The heatmap was generated using Cluster 3.0 program based on Euclidean similarity and average hierarchical linkage.

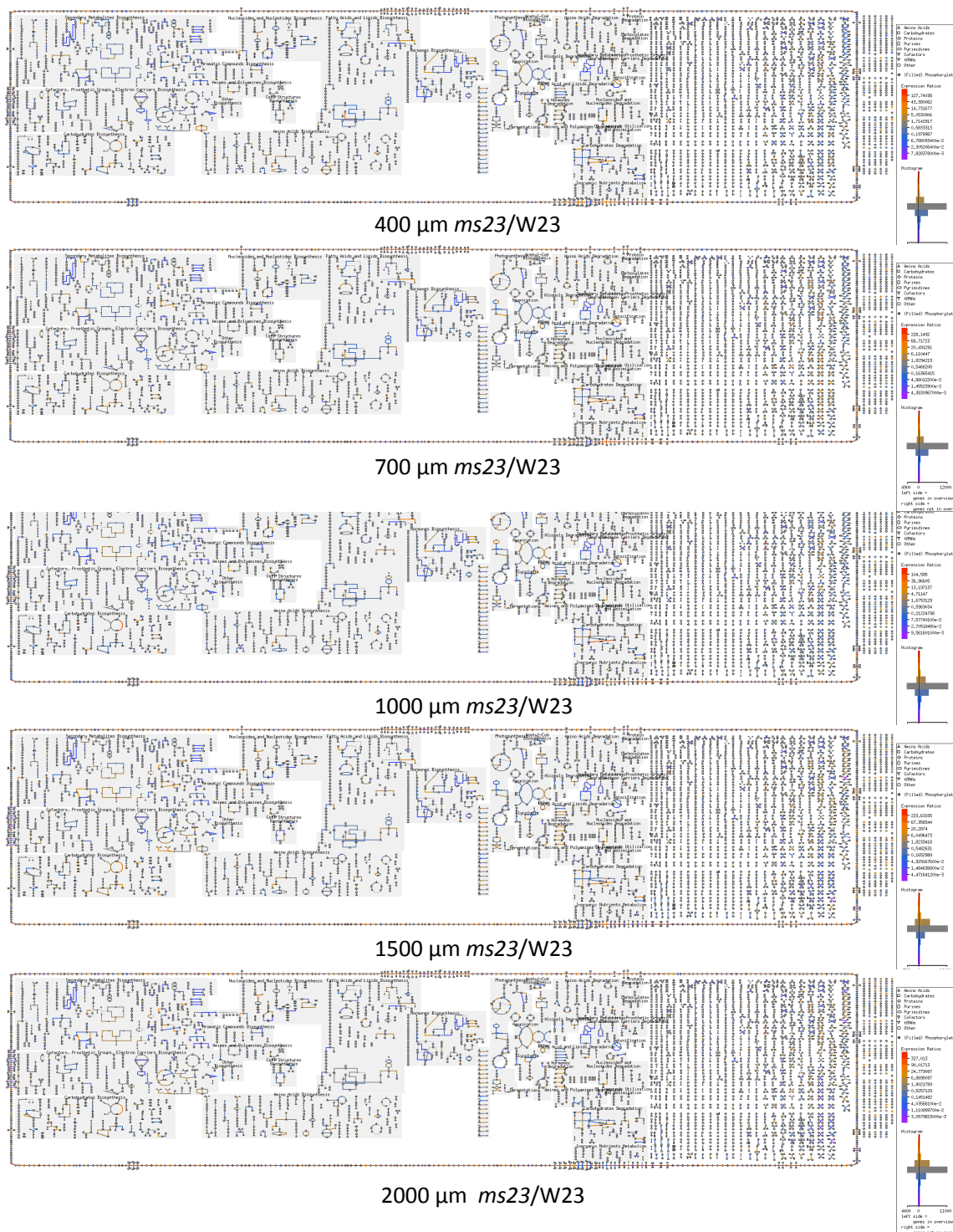


Fig. S12. Pathway mapping using the transcriptomic analysis tool (<http://pathway.gemene.org/maizecyc.html>) comparing *ms23-ref* and the *W23* fertile inbred at the 400-, 700-, 1,000-, 1,500-, and 2,000- μm stages based on RNA-seq. Data are from the Gene Expression Omnibus (GEO) database, www.ncbi.nlm.nih.gov/geo (accession nos. GSE52290 described in Zhai et al., 2015).

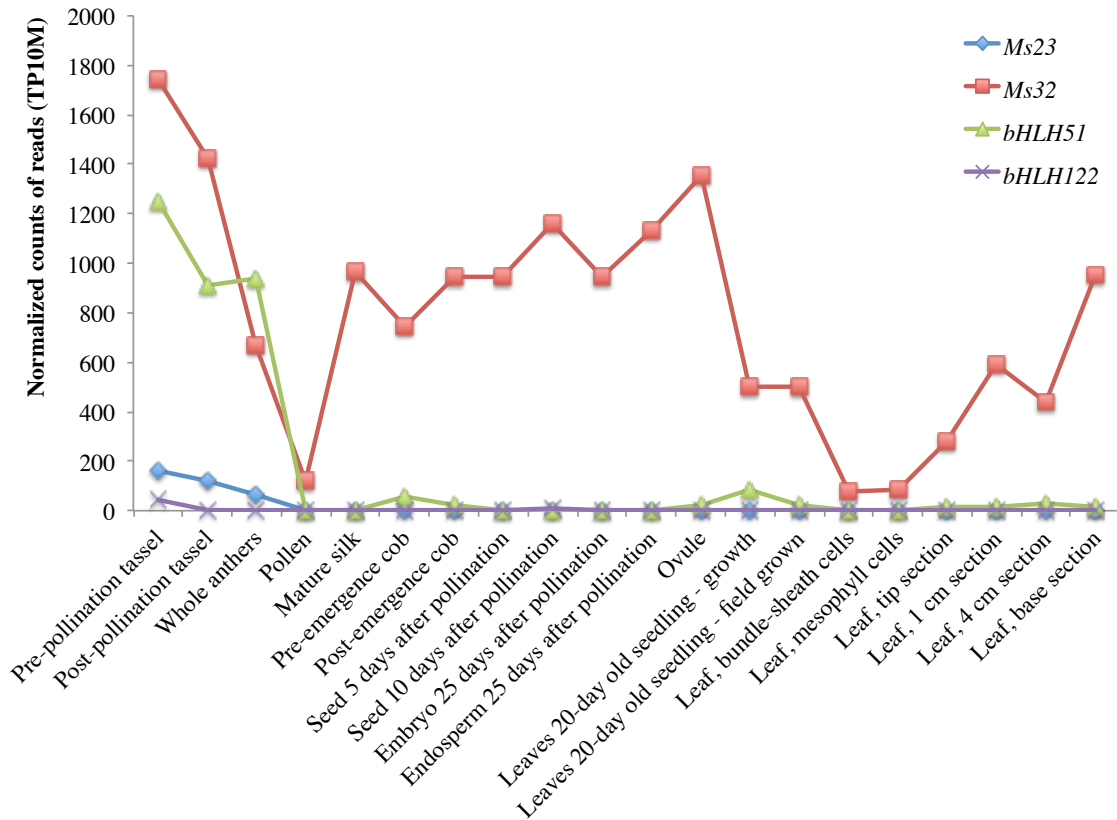


Fig. S13. Expression patterns of *Ms23*, *Ms32*, *bHLH51*, and *bHLH122* in various organs. Normalized sum of abundances from twenty vegetative and reproductive tissues across a wide range of developmental stages were compiled from published RNA-seq data. The total counts of RNA-seq reads in each gene model are normalized to 10 million reads (TP10M) (https://mpss.danforthcenter.org/dbs/index.php?SITE=maize_RNAseq).

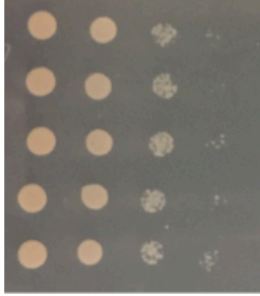
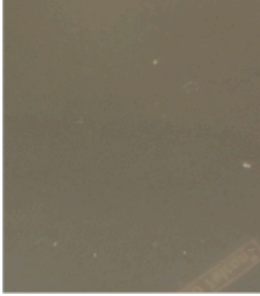



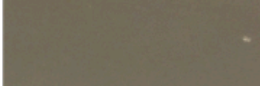



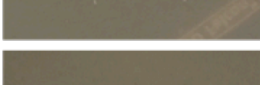



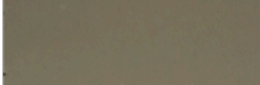



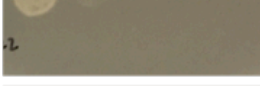

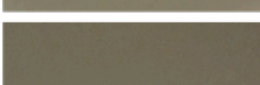



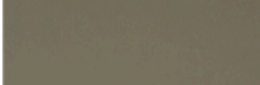









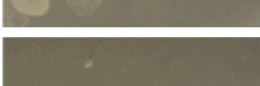


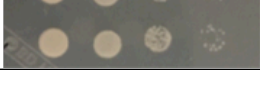
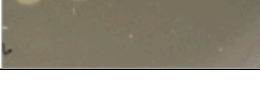
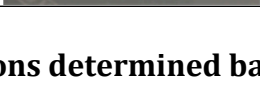
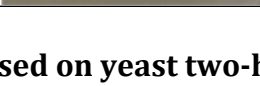
Bait	Prey	Low Stringency	High Stringency	Interaction
Empty	Empty			No
Empty	MS23			No
Empty	MS32			No
Empty	bHLH51			No
Empty	bHLH122			No
MS23	Empty			No
MS23	MS23			No
MS23	MS32			No
MS23	bHLH51			Yes
MS23	bHLH122			No
MS32	Empty			No
MS32	MS32			No
MS32	bHLH51			No
MS32	bHLH122			Yes
MS51	Empty			No
bHLH51	bHLH51			Yes
bHLH51	bHLH122			Yes
bHLH122	Empty			No
bHLH122	bHLH51			Yes
bHLH122	bHLH122			No

Fig. S14. Protein interactions determined based on yeast two-hybrid assays.

Serial dilutions (1, 10^{-1} , 10^{-2} , 10^{-3}) of yeast two-hybrid clones under low (-Leu, -Thr) and high (-Leu,-Thr,-His, -Ala) stringency conditions. Each bait and prey vector contains a bHLH domain from MS23, MS32, bHLH51, or bHLH122. Empty bait (pGBK) and empty prey (pGAD) were used as negative controls.

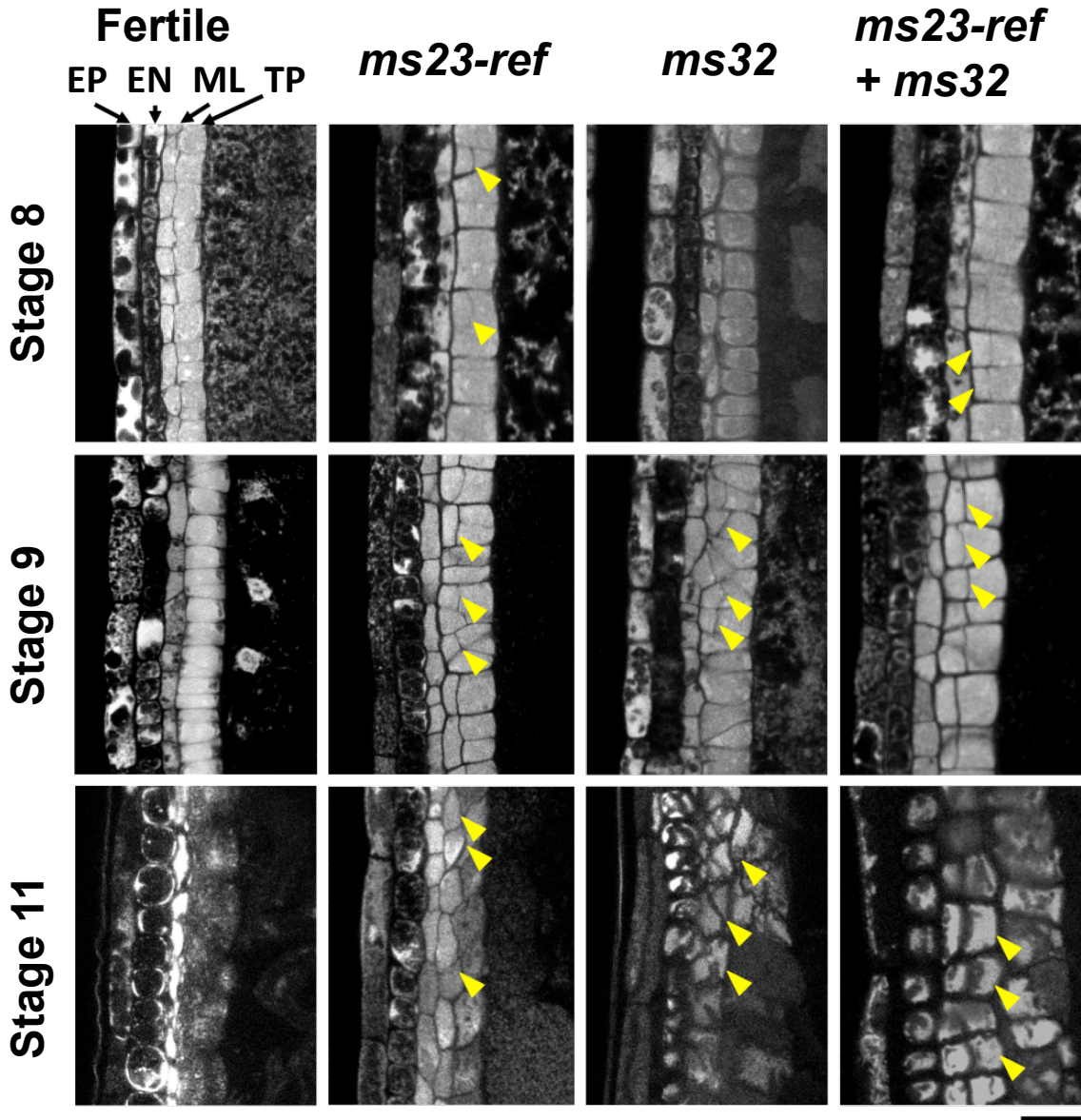


Fig. S15. Longitudinal confocal images of *ms23-ref*, *ms32*, and the *ms23-ref*, *ms32* double mutant at three developmental stages. Yellow triangles point to cells produced by extra periclinal divisions. Scale bar: 20 μ m

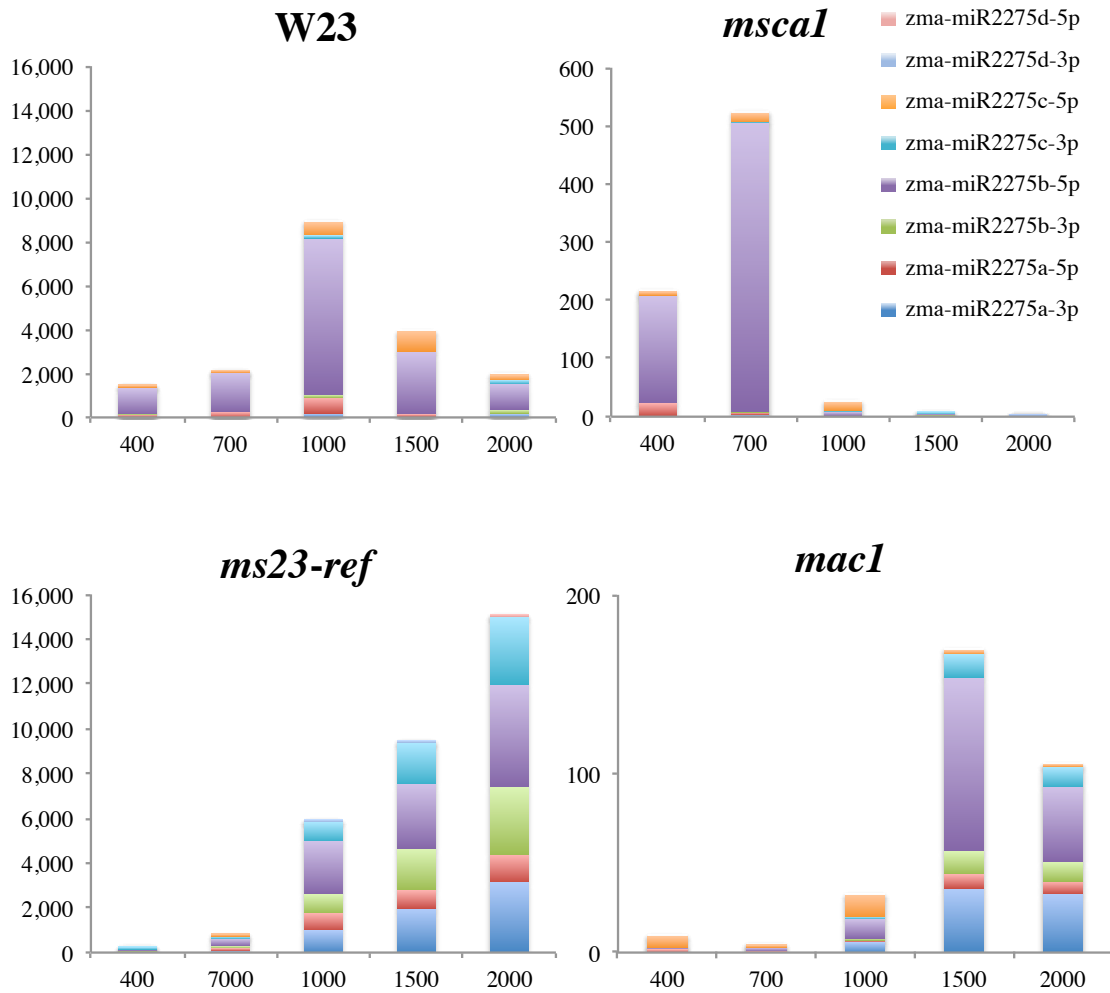


Fig. S16. miR2275 abundances in W23, *ms23-ref*, *msca1*, and *mac1* anthers based on small RNA-seq data. (A) The miR2275 profiles of 0.4-, 0.7-, 1.0-, 1.5-, and 2.0-mm anthers of homozygous *ms23-ref*, *msca1*, and *mac1* mutants comparing to the W23 fertile line. The total counts of RNA-seq reads are normalized to 10 million reads (TP10M) (Zhai et al., 2015).

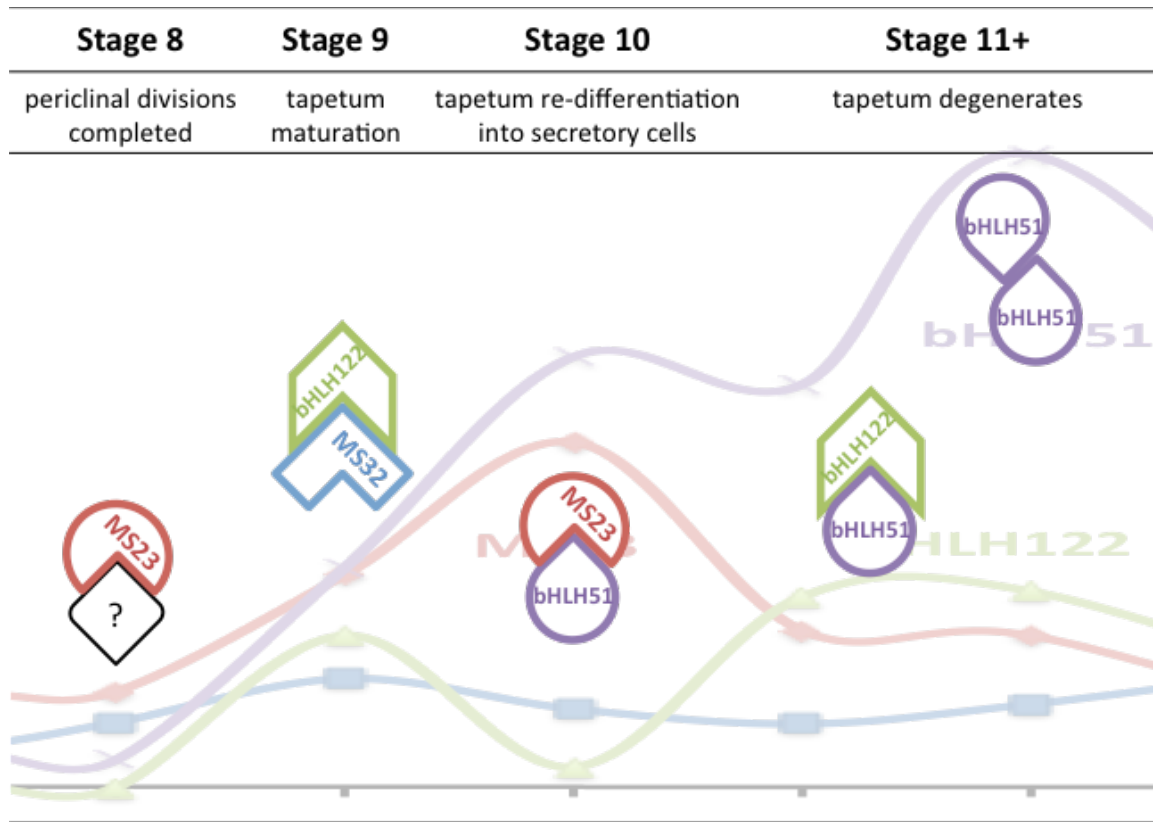


Fig. S17. A proposed “partner exchange” model of sequential steps of tapetal differentiation in maize. We propose that MS23 prevents periclinal division, likely as a heterodimer with an unknown factor to regulate the last periclinal division in the SPC and the pre-tapetal cells during their anticlinal proliferation in Stage 8. The MS23:unknown factor complex is required for tapetal cell fate. The MS32:bHLH122 complex acts to prevent excessive, aberrant divisions beyond Stage 9 after most tapetal cells are formed. The absence of bHLH122 at Stage 10 facilitates another partner exchange in which newly synthesized bHLH51 can interact with MS23, critical for the re-differentiation of the TP to serve its secretory roles at Stage 10. With bHLH122 reappears and MS23 levels off at Stage 11, bHLH51 is released to form new complexes (bHLH51:bHLH122 and bHLH51:bHLH51) for the post-meiotic, late development of the TP, e.g., tetrad callose dissolution, exine deposition onto pollen, maturation of somatic walls to permit pollen attachment, and ultimately programmed cell death of the TP.

Table S1. Comparison of the amino acid identity to MS23 with twelve other bHLH proteins important for tapetal functions in maize, rice, and Arabidopsis anthers.
MS23 protein sequence was used as the basis for the comparison.

Protein Name (species)	Total length (amino acids)	Amino acid identity (%)	bHLH domain identity (%)
MS23 (<i>Zea mays</i>)	365	100.00	100.00
TIP2 (<i>Oryza sativa</i>)	379	72.68	91.11
bHLH122 (<i>Zea mays</i>)	491	27.38	52.27
EAT1/DTD (<i>Oryza sativa</i>)	464	26.36	50.00
bHLH91 (<i>Arabidopsis thaliana</i>)	428	25.43	46.67
bHLH89 (<i>Arabidopsis thaliana</i>)	420	26.43	42.22
bHLH10 (<i>Arabidopsis thaliana</i>)	458	26.21	42.22
bHLH51 (<i>Zea mays</i>)	625	13.93	42.22
TDR (<i>Oryza sativa</i>)	551	14.12	42.22
AMS (<i>Arabidopsis thaliana</i>)	571	12.75	42.22
DYT1 (<i>Arabidopsis thaliana</i>)	207	19.25	37.78
MS32 (<i>Zea mays</i>)	219	15.46	35.56
UDT1 (<i>Oryza sativa</i>)	177	20.12	37.78

Table S2

[Click here to Download Table S2](#)

Table S3

[Click here to Download Table S3](#)

Table S4

[Click here to Download Table S4](#)

Table S5

[Click here to Download Table S5](#)

Table S6. Anther stages in maize, rice, and Arabidopsis. Based on the developmental events previously defined (Kelliher et al., 2014; Sanders et al., 1999; Zhang and Wilson, 2009), anther stages in maize, rice, and Arabidopsis are compared and listed. AR – archesporial; EN – endothecium; SPC – secondary parietal cell; PMC – pollen mother cells.

Events	Anther stages		
	Maize	Rice	Arabidopsis
Pluripotent primordium	1	1	1
AR cells forming	2	2	2
EN and SPC forming	3	3	3
Three-wall-layer stage with EN and SPC complete	4	4	3-4
SPC periclinal divisions starts	5	4	4
Anticlinal divisions to add anther girth	6	4	4
Final SPC periclinal divisions	7	4	4-5
AR cells mature to PMC	8	5	5
Meiosis starts	9	6	5-6
Entering Meiosis II	10	7	6-7
Meiosis complete	11	8	7

Tables S7 – S9

[Click here to Download Tables S7 - S9](#)